THE ARUP JOURNAL

DECEMBER 1983

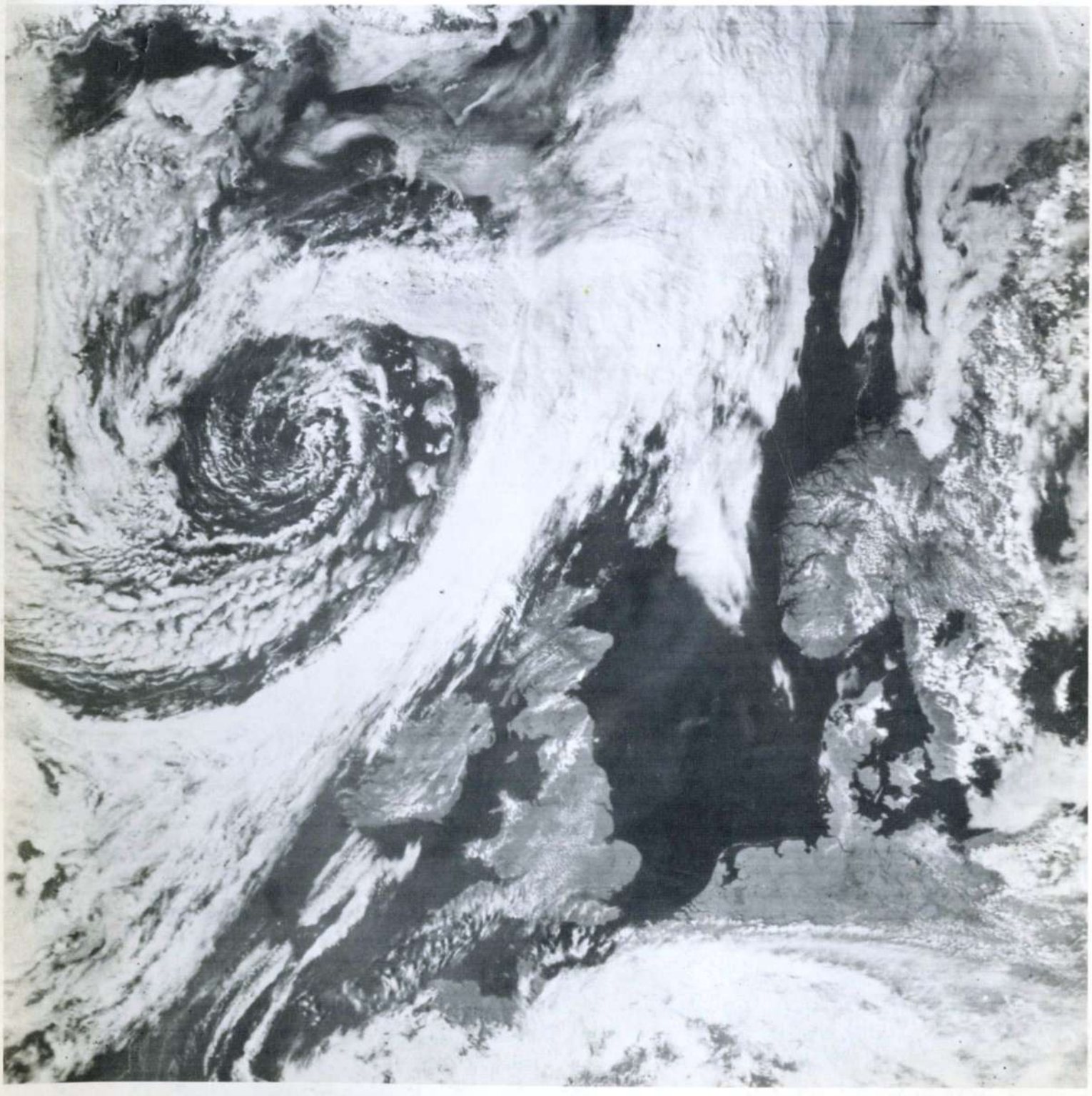

THE ARUP JOURNAL

Vol. 18 No. 4 December 1983
Published by
Ove Arup Partnership
13 Fitzroy Street, London W1P 6BQ

Editor: Peter Hoggett
Art Editor: Desmond Wyeth FSIAD
Assistant Editor: David Brown

Contents

Front cover: Cold front approaching Britain (Photo: University of Dundee)
Back cover: The Hong Kong tunnel (Photo: Neil Farrin)

The seawater intake system for the new headquarters of the Hongkong and Shanghai Banking Corporation

Architect: Foster Associates

Simon Murray

Introduction

The new headquarters for the Hongkong and Shanghai Banking Corporation at 1 Queen's Road Central, Hong Kong, needs no introduction. Much has been written about the design of the building which will replace one of Hong Kong's most significant landmarks. At the time of writing the structure has risen almost to the level of the surrounding buildings.

The original headquarters was supplied with seawater for both cooling and flushing. The seawater was drawn from an intake chamber built behind the seawall some 400m from the bank. It was pumped to the site through two 400mm mains laid in a trench below the surface of Statue Square. When the time came to redevelop the site it was hoped that a similar system could be developed for the new building.

Early in 1981 the professional team, led by the architect Foster Associates, began to investigate the feasibility of supplying seawater to the new development. A variety of solutions were appraised starting with the renovation of the existing system. The study concluded that the optimum solution was to lay the seawater mains in a tunnel excavated beneath Statue Square and to distribute the capital cost of the works by sharing the system with other developments.

The proposal which the architect put to the client in December 1981 was to construct a new intake and pumphouse close to the original installation. The seawater was to be carried to the new development in six 1m diameter pipes laid in a tunnel excavated at an average depth of 60m below Statue Square. The system was designed with a capacity of 4000 l/sec of which approximately 3000 l/sec was intended for other developments. The proposal was accepted and in January 1982 Ove Arup and Partners (Hong Kong) were appointed to lead the professional team in its implementation.

The programme for the commissioning of the air-conditioning equipment in the new headquarters building required that seawater be available in August 1984. This gave the team a period of only 32 months for the design, construction and commissioning of the seawater system. Failure to meet this programme could delay the opening of the building.

To resolve the programme the construction work was divided between two contracts. The first contract comprised the design and construction of an access shaft adjacent to the seawall. It was awarded to Bachy Soletanche Group in May 1982 and, while it was under construction, the team proceeded with the design and documentation of the remainder of the system. The management contractor invited four civil engineering contractors to tender for the major contract. In November 1982 it was awarded to Aoki Construction Company Ltd. who sub-contracted the mechanical and electrical works to Haden International Ltd.

Shortly after the award of the main contract it became apparent that Hong Kong's economy had passed its peak of expansion and had entered a decline. The subsequent loss in confidence in the property market had serious consequences for the project. It led to the withdrawal of the other users of the system who were to have taken 75% of its capacity. Construction was already under way and the team carried out a swift evaluation of the options available to the client. The client elected to proceed with the construction of the full civil engineering works but to install within them a seawater system with only sufficient capacity for the new bank headquarters. The seawater pipework was to be confined to one half of the tunnel leaving the other half available for the installation of pipework to serve other sites as and when they are developed.

At the time of writing the seawater system has been redesigned, the civil engineering works are under construction and the mechanical and electrical equipment is being ordered.

The seawater system

The arrangement of the seawater system is shown in outline in Fig. 1. A fundamental principle of the design is that every piece of plant and pipework in the system is provided with a backup unit. This ensures that the new bank headquarters can continue to operate under all conditions.

Seawater is drawn from the harbour through a forebay unit set in the seawall. The water passes into the intake chamber located behind the seawall and thence into the two 900mm diameter intake pipes which are cast into the rear of the chamber. This somewhat elaborate intake design is necessary to overcome the fact that at low tide the water depth at the seawall is less than 1m.

The centre of the system is Shaft No. 2 which serves as both a pumphouse and a means of access to the tunnel. The two intake pipes enter the shaft 7m below ground level and turn through 90 degrees to form the two intake stacks. The three identical pump sets are connected between the intake stacks and the delivery stacks at three separate floor levels. From the lowest level delivery pipes continue down the shaft and into the tunnel.

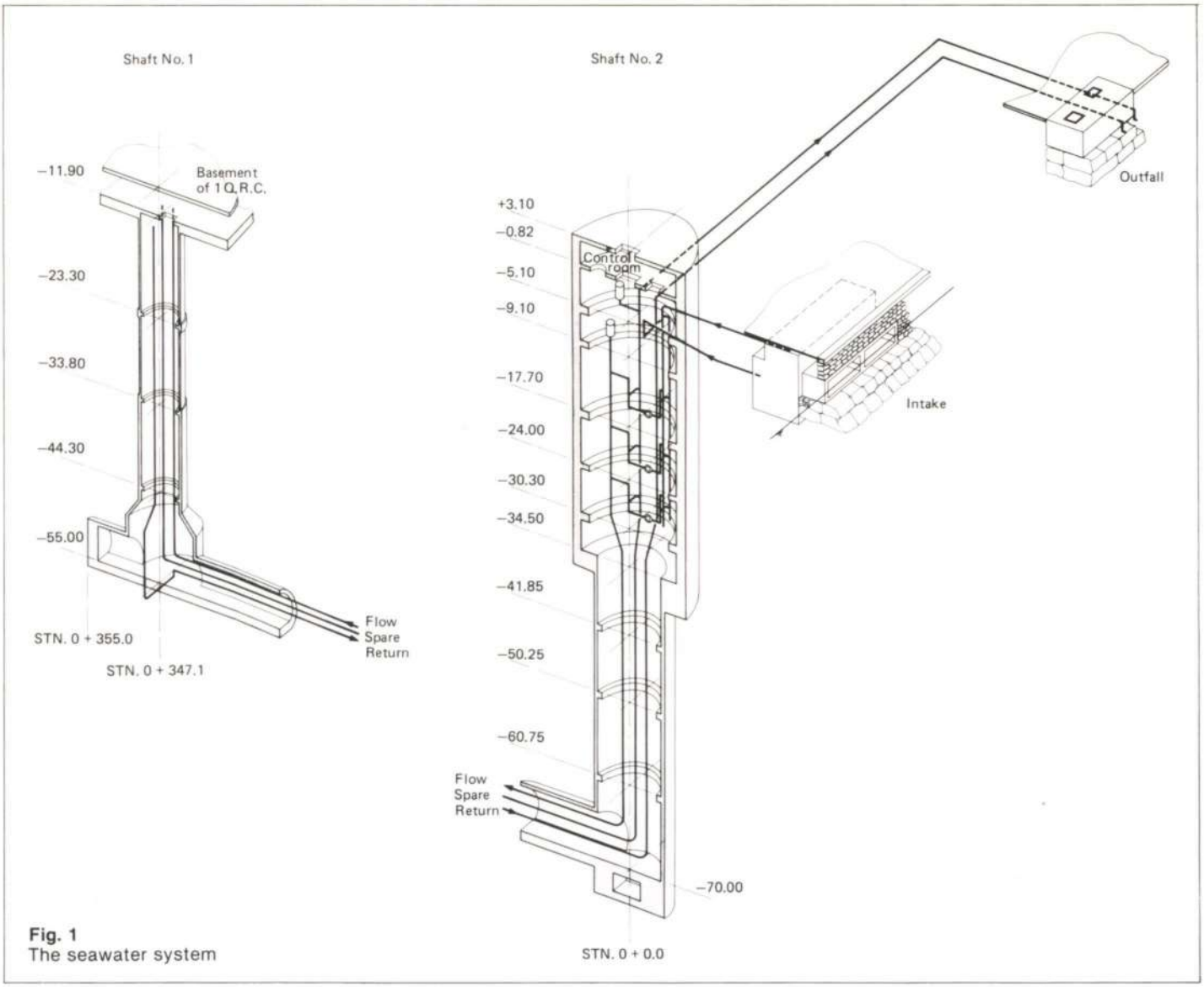

Fig. 1
The seawater system

Fig. 2
The tunnel alignment (Photo: Neil Farrin)

The upper half of the shaft, which houses all of the plant, is 12m in diameter and has an overall depth of 40m. The top two levels in the shaft are set aside for transformers, electrical switchgear, ventilation equipment and control equipment.

The tunnel (Fig. 2) is the conduit for both the flow and return pipework. In this closed loop the requirement for full standby capacity is met through the use of three 700m diameter seawater pipes: one flow, one return and one spare pipe which can be flow or return. The three pipes are carried 350m along the tunnel to a point in the ground 40m below the basement of the building. The pipes rise into the basement through Shaft No. 1.

The return pipe follows the same route as the flow pipe. At the top of Shaft No. 2 the return pipes are taken out through the shaft wall and are carried in trench to the old intake chamber which served the original headquarters building. The chamber is located in the Star Ferry concourse and is a concrete box set behind the seawall. Once stripped of its existing pumps and pipework it provides a convenient outfall chamber. The outfall pipes pass through the seawall within the chamber and then discharge into the sea below the Star Ferry Pier.

Access for maintenance is a critical aspect of the design of the system. Access for personnel is by industrial hoist with cat-ladders provided for emergencies. Vertical plant access zones are provided in both shafts and are connected by a horizontal access zone in the tunnel giving an unrestricted continuous space for the movement of plant and equipment.

The basic dimensions and characteristics of the seawater system are as follows:

Intake temperature:	28°
Outfall temperature:	34°
Flow rate:	1000 l/sec
Cooling capacity:	5500 tonne refrigeration
Seawater pipes:	700mm diameter class K9 ductile iron pipes with cement mortar lining.
Seawater pumps:	Three 270 kW double volute centrifugal pumps each delivering 500 l/sec at 350 kPa.

The support of the seawater pipes

The function of the civil engineering works is to provide space and support for the pipework and plant. The behaviour in service of the pipework and plant is largely determined by the manner in which it is supported. One of the first exercises to be undertaken in the design was the development of a method of supporting the vertical pipe stacks in the two shafts.

The loads acting on the seawater pipes originate from the mass of the pipes themselves and from the thrusts induced at bends and fittings by the water pressures acting inside the pipes. In this system the weight of the pipes is insignificant in comparison with the thrusts under surge conditions.

The design of the support system was dictated by maintenance procedures. The support system had to permit any length of pipe to be released and replaced without affecting the rest of the system. The system which evolved is shown in Fig. 3. The vertical pipe stacks are divided into discrete lengths by socket joints immediately above each support floor. The length of pipe beneath the socket is supported in a steel collar which is in turn carried on the steel floor beams. Hydraulic jacks between the collar and the socket allow any length of pipe to be moved vertically relative to the rest of the system. To replace a fitting within the stack one would release the flanges either side of it and then jack the stack away from it, allowing it to be removed. The new fitting would be inserted by the reverse process.

The vertical forces acting in the pipe stacks are carried into the steel floor beams through the collar located immediately above the point of action of the force. The steel floor beams span between reinforced concrete waling beams cast into the shaft linings. Items of plant such as pumps and surge vessels are supported on secondary beams spanning between the primary floor beams.

Within the tunnel the seawater pipes are supported on simple steel frames bolted to the tunnel lining (Fig. 4). The pipework in the tunnel is socket jointed at 5.5m intervals and the frames are spaced to lie immediately behind each set of sockets. The frames are tied together with tie rods and turnbuckles to resist the longitudinal thrusts in the pipes.

Planning of the underground works

The first stage in the planning of an underground excavation is to understand the geological origins of the strata in which it will be built. Central District of Hong Kong Island is underlain by Hong Kong Granite which forms one large intrusion centred in the harbour and exposed in the northern part of Hong Kong Island, Kowloon and Kwun Tong.

The tunnel alignment lies below reclaimed land within the natural harbour (Fig. 5). As a result of its protection from the erosive force of the sea, the rock in this area is overlain by a considerable thickness of completely decomposed granite (CDG), The CDG is in turn overlain by recent marine sediments and reclaim fill. In the reclaim fill the water table follows the tide. In the other strata the piezometric levels are generally at + 1.0 mPD.

The general level of the tunnel was dictated by two factors. The presence of Chater Station, constructed through the CDG to rockhead and running perpendicular to the horizontal alignment of the tunnel, precluded the use of a shallow soft ground tunnel. The relatively short time available for the construction of the tunnel required that it be excavated by simple drill and blast techniques in rock which required minimal primary support.

The approximate vertical alignment of the tunnel was defined using information from preliminary site investigations and geological surveys. When this had been done a final site investigation was carried out to define the precise vertical alignment and to provide the reference conditions required for the management of the civil engineering contract. In planning the final site investigation the object was to obtain sufficient information on rock mass quality to assess the need for primary support along the length of the tunnel. Several methods of rock mass classification were considered and that finally selected was a simple system based on the degree of weathering of the rock mass. This system, which has been described by Ruxton and Berry divides the rock mass into zones based on its appearance in exposures and cores and on a visual assessment of its engineering properties.

The design of the horizontal alignment of the tunnel (Fig. 2) was relatively simple. The vertical alignment was more complicated and was essentially an exercise in balancing several incompatible factors to produce a tunnel which could be constructed by conventional means in the time available. Perhaps the single most important factor was that the contractor would have access only from Shaft No. 2. To simplify ground water control during construction the alignment was graded towards Shaft No. 2 although the gradient was limited by the need to be able to operate vehicles for the removal of muck from the excavation. The level of the tunnel was dictated by the preliminary support design and was generally set to maintain a 'cover' of 6m of Zone D granite over the crown of the excavation.

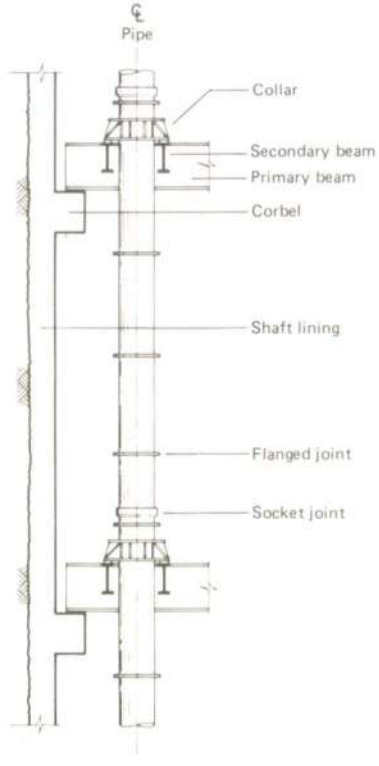

Fig. 3
The pipe support system in the shafts

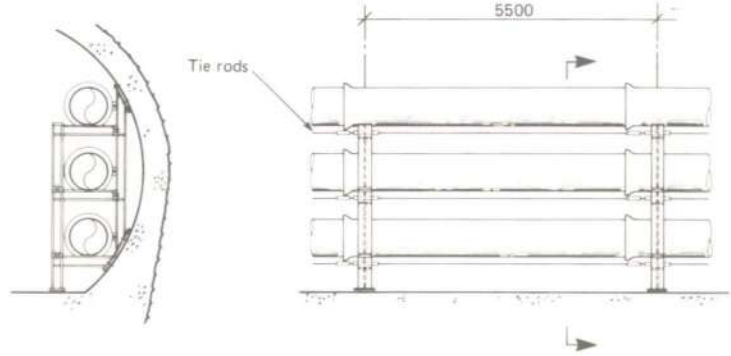

Fig. 4
The pipe support system in the tunnels

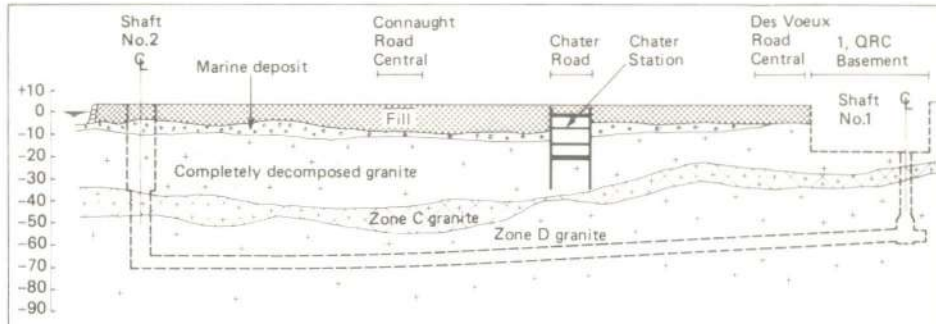

Fig. 5
Geological section through the underground works

At the planning stage the need for secondary linings was assessed and outline specifications were prepared for their design. As the tunnel and shaft excavations were designed to be self-supporting the primary function of the secondary linings was to control the flow of groundwater into the permanent works. Investigations showed that the optimum solution for both shafts and tunnel was a cast in situ concrete lining constructed after completion of the excavation.

The final stage in the planning of the underground works was to confirm that the shafts and tunnel could be constructed in the time available in the overall programme. This exercise was carried out by the construction management consultants Bush and Rennie International who prepared an indicative construction method statement and programme.

Design of Shaft No. 2

The design of the upper half of Shaft No. 2 was a geometrical problem. The site was constrained on all four sides by existing services and the City Hall Memorial Gardens (Figs. 6 and 7). Calculations had shown that if the diaphragm wall could be constructed in a circle the external pressures from the soil and water could be carried in ring compression within the wall section. If the layout of the shaft deviated too far from a circle it would be necessary to construct horizontal diaphragms within the shaft to support the wall panels.

Armed with the dimensions of standard diaphragm wall grabs, the design team set out to demonstrate that it was feasible to construct a circular diaphragm wall with an internal diameter of only 12.0m. Before long it was clear that the solution would vary from contractor to contractor depending on the size of their equipment. The obvious solution was to invite contractors to submit tenders for the design and construction of the shaft.

Tenders were invited on the basis of geometrical limits and a performance specification. The contract was awarded to Bachy Soletanche Group who proposed a circular shaft constructed from 1.2m thick diaphragm wall panels (Fig. 7). The shaft required no internal horizontal supports provided that it was constructed as a circle. There was concern that if the diaphragm wall panels were not vertical the horizontal section at the base of the shaft could deviate so far from a circle as to invalidate the assumption of pure ring compression. This led to a requirement that the wall panels be constructed to a vertical tolerance of 1/160.

Waling beams are required in Shaft No. 2 for the support of the steel floor beams. In addition a transition collar is provided at rockhead to reduce the diameter of the shaft to 8m. Both of these elements were designed as conventional reinforced concrete members connected to the diaphragm wall panels by reinforcing bars bent out from the main cages.

Design of the tunnel lining

The primary function of the tunnel lining is to reduce to an acceptable level the flow of water into the permanent works. Its secondary function is to support the pipes and other services contained within it.

The first stage in the design of the tunnel section (Fig. 8) was to define the space required within it. In the original system the arrangement of the seawater pipes was dictated by the method of installing them. The management contractor advised the design team that if the pipes were to be installed within the time available it was essential that they were stacked either side of an unrestricted access way.

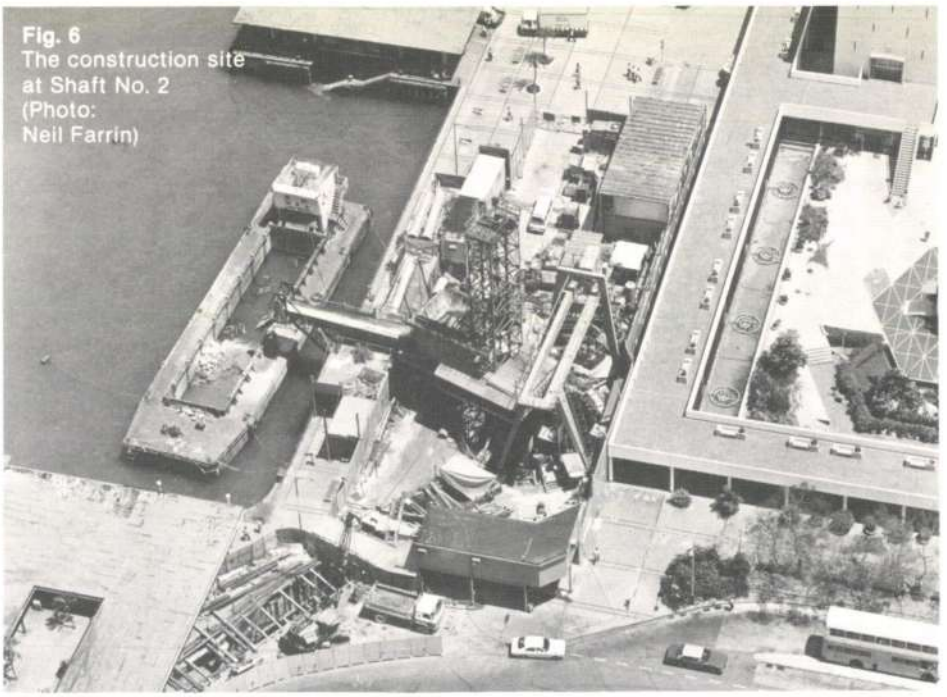

Fig. 6
The construction site at Shaft No. 2 (Photo: Neil Farrin)

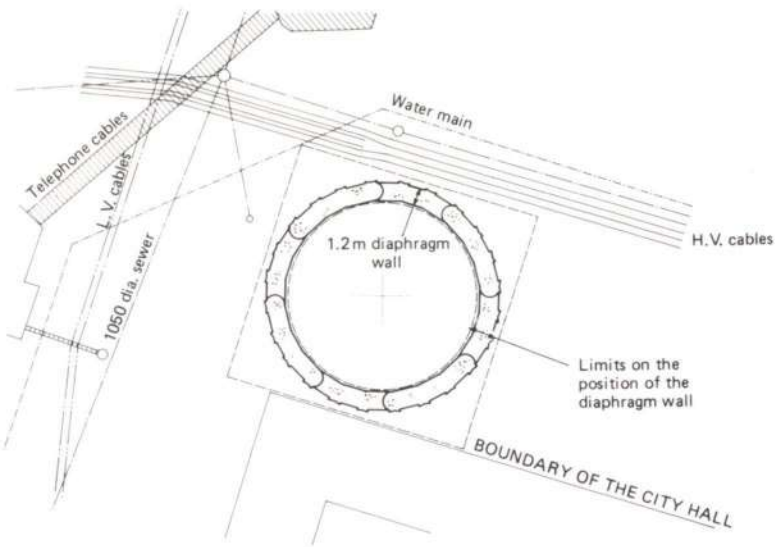

Fig. 7
Constraints on the location of Shaft No. 2

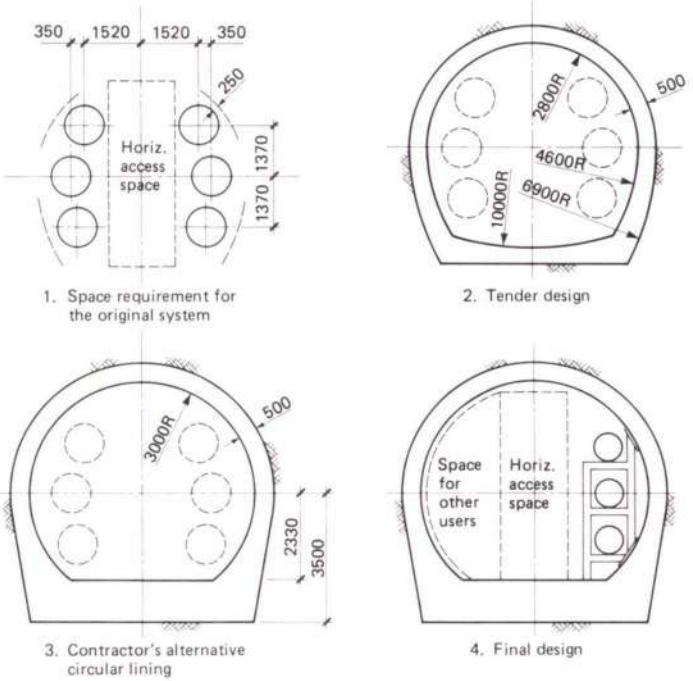

Fig. 8
The development of the tunnel lining

Fig. 9
Shaft No 2: Concreting a diaphragm wall panel

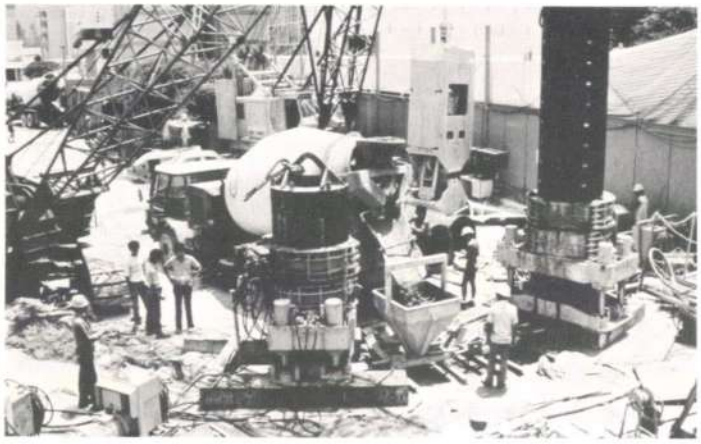

Fig. 10
Shaft No 2: Construction of a waling beam

12

Fig. 11
Shaft No 2: The start of excavation

Fig. 12
Shaft No 2: The upper section

Fig. 13
Excavation of a top heading in the tunnel

Fig. 14
Drilling charge holes with an air leg drill

11

13

14

At the design stage several alternative tunnel sections were investigated. The objective was to design a lining section which contained the minimum volume of excavation, required little or no reinforcement and provided the contractor with a flat invert in the excavation to act as a roadway during construction. The tender design (Fig. 8) was a horseshoe section with reinforced invert slab and an unreinforced arch.

Having been awarded the sub-contract the contractor proposed that the tunnel lining be changed to an unreinforced circular section. The contractor considered that the increase in the volumes of excavation and concrete were more than balanced by the elimination of the reinforcement in the invert slab. The contractor's proposal was evaluated and has been adopted. The layout of the services within the tunnel has been redesigned for the reduced mechanical system.

The construction of Shaft No. 2

The construction of the diaphragm wall for the upper half of Shaft No. 2 commenced in May 1982 and was completed in February 1983. It was a routine exercise in diaphragm wall construction, starting with the drilling of prebores to define the final depth of each panel and ending with the excavation and concreting of the final panel.

The key to the safe construction of diaphragm walls in sensitive areas is an effective system of monitoring and analyzing the response of the ground to the excavation of each panel. At Shaft No. 2 the excess head of bentonite within the panel being excavated was maintained by dewatering from wells inside the shaft. Piezometers were installed in the CDG around the wall panels to ensure that the head was maintained without excessive drawdown. Inclinometers were installed adjacent to critical panels to monitor the lateral movement of the ground during panel excavation.

The monitoring of ground surface settlement points showed that during the concreting of the primary panels the ground nearby settled by up to 75mm. Investigation showed that this was caused by the removal of the 40m long stop-end tubes as the concrete was poured. (Fig. 9). The jacks used to lift the tubes were exerting very large reactions on the guide walls and effectively jacking them into the ground. Once recognized, the problem was solved by careful control of the jacking operation.

On completion of the diaphragm wall panels, the toe of the wall was grouted through tubes cast into the panels and boreholes drilled around the outside of the wall. The object of this exercise was to create a seal between the bottom of the wall and the underlying bedrock. A pump test was carried out to confirm that the completed wall met the requirements of the performance specification and all was then ready for the shaft to be excavated.

The excavation of the shaft was an exciting time on site. For the first time the team could see the strata which hitherto had been obscured with bentonite. The excavation commenced with the breaking out of the inner guide wall (Fig. 10). A hydraulic excavator was then placed in the shaft to dig the soil and load it into skips to be lifted to the surface. As each waling beam level was reached the excavation was temporarily halted, the connecting reinforcement bent out from the diaphragm wall and the waling beam cast (Fig. 11).

After 12 weeks of excavation the toes of the diaphragm wall panels were finally reached. The exposed rock surface was cleaned and a large concrete collar formed on it to define the transition to the lower half of the shaft. The upper half of Shaft No. 2 was complete (Fig. 12).

The construction of the tunnel

Aoki Construction Company Ltd. moved onto site in February 1983. Their first task was to establish the site infrastructure necessary for the shaft sinking and tunnelling works (Fig. 6). The key to the planning of the infrastructure was the method of removing broken rock from the underground works. The sub-contractor installed a skip system in Shaft No. 2. The skip is hoisted on guide rails by a winch housed in a headgear at the top of the shaft. The skip discharges into a holding bin at surface. From the bin the rock is carried by conveyor to a barge moored adjacent to the site.

The lower section of Shaft No. 2 was sunk by drill and blast techniques to its final depth of 80m. Shot holes were drilled with hand-operated air leg drills. After the blast the muck was loaded into the skip with a small hydraulic excavator.

When the excavation reached the shaft invert a 20m length of tunnel was driven to create space for the establishment of the

Charged holes: 125
Relief holes: NIL
Drilled length: 1.8 – 2.4 m
Total explosives: 90kg
Max. per delay: 9kg

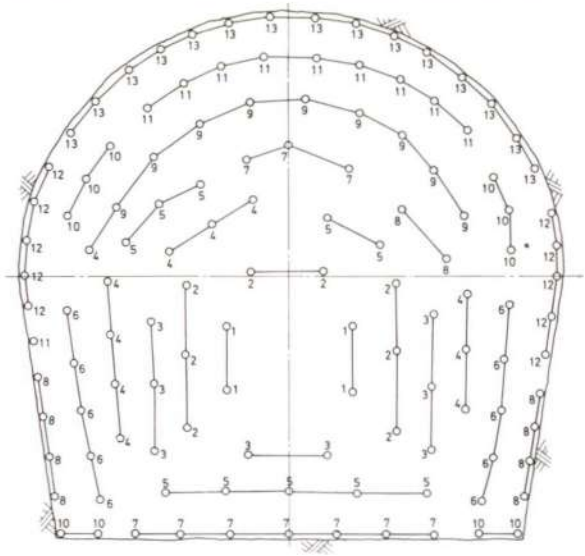

Fig. 15
Blasting pattern for tunnel excavation

Fig. 17
LHD and muck skip
at the base of Shaft No 2

(Photos: **9-12**, Simon Murray.
13-14, Alan Kemp. **16**, Warren Beynon)

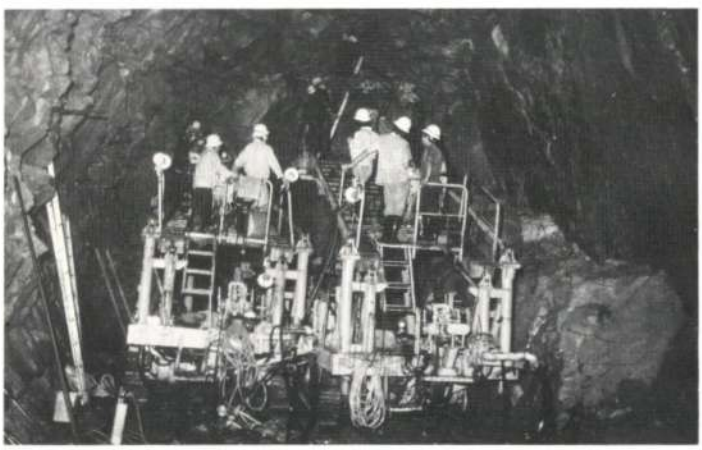

Fig. 16
Drill jumbos in the tunnel

Fig. 18
The tunnel excavation

sub-contractor's underground plant. This length of tunnel was excavated in two stages. First a top heading was excavated in the upper half of the tunnel section (Fig. 13). The bench in the lower half of the section was then removed.

The main tunnel excavation is being carried out by drilling and blasting full face. Each cycle of excavation commences with the setting out on the face of the pattern of 125 charge holes (Fig. 15). The arrangement of holes, the charge in each and the sequence of detonation is designed to remove and fragment the required amount of rock with the minimum of overbreak. The sequencing of detonations using standard delays ensures that the energy transmitted into the ground is spread over a period of several seconds, thereby minimizing the vibration levels experienced at ground surface.

The charge holes are drilled with two three-boom jumbos (Fig. 16). These machines are tracked platforms on which are mounted three hydraulically-positioned drills. The platforms are large enough to allow the drills to reach all parts of the face. The drills themselves are considerably more powerful than the alternative hand-operated drills and can achieve much faster drilling rates.

After the holes have been charged and the round fired, the face is ventilated to remove residual gases. Access can then be gained for barring down loose rock to make safe the area around the muck pile. Mucking out is being done with an LHD (Fig. 17). This rubber-tyred excavator loads the broken rock and transports it to a temporary stockpile at the base of the shaft. A crawler loader transfers the rock from the stockpile into the skip for hoisting to surface.

To date the primary support in the tunnel excavation has been limited to occasional rock bolts required to stabilize individual rock wedges. Steel sets are kept on site in case they are needed for the support of localized zones of highly weathered rock.

In the excavation of a tunnel in these conditions it is important to investigate the ground ahead of the face to detect potential hazards before they are exposed. At approximately weekly intervals three horizontal probe holes are drilled a depth of 20m into the face. The rates of penetration of the drill bits are measured as a comparative indication of the strength of the rock mass. The rates of flow of water out of the probe holes are also recorded. Where significant flows of water are encountered, the ground ahead of the face is grouted before being excavated.

Future work

At the time of writing, the tunnel face is 150m from Shaft No. 2. A further 205m of tunnel remain to be excavated. It is intended that the basic method of excavation will be unchanged although the mucking operations will be affected by the increasing haulage distances and steeper gradients as the excavation approaches Shaft No. 1.

Shaft No. 1 is planned to be excavated in two operations. The sub-contractor responsible for the construction of the basement will sink the shaft to a depth of about 15m below basement level. The sub-contractor for the seawater system will then raise the remaining 20m of shaft from the tunnel. The relatively small height of the raise precludes the use of sophisticated boring equipment. It is probable that the raise will be executed by drill and blast using a simple climbing stage for access.

On completion of the excavation the shafts and tunnel will be lined with cast in situ concrete linings and the mechanical and electrical works will be installed. The system is programmed to be completed in September 1984.

Acknowledgements

Douglas Parkes for his advice and assistance in the planning of the underground works.

Neil Farrin, Merete Henrichsen, O Y Kwan, Chris Nunns, Can Wong and W P Yeung for their contributions to the preparation of this paper.

Credits

Client:
1 Queens Road Central Ltd.

Architect:
Foster Associates

Mechanical and electrical consultants:
J Roger Preston & Partners

Quantity surveyors:
Levett & Bailey

Management contractor:
John Lok/Wimpey Joint Venture

Sub-contractors:
Bachy Soletanche Group
Aoki Construction Company Ltd.
Haden International Ltd.

Seminar on wind effects on buildings

These two papers by David Croft and Michael Willford formed part of the above Ove Arup Partnership seminar, held in London in May 1983

Surface pressures

David Croft

SYNOPSIS

In this paper the general pattern of wind flow around buildings is discussed briefly and some of the difficulties with the use of pressure coefficients identified.

Most of the paper, however, is concerned with wind tunnel testing, in particular the need to specify the test properly and to interpret the results correctly, if meaningful design values are to be obtained. To this end some statistical theory is presented.

During the last year a number of wind tunnel tests have been carried out for various parts of the firm. One such test is described in detail and is used to illustrate the various statistical concepts.

The treatment of internal pressures is discussed, somewhat inconclusively, and the various other aspects that should be considered when determining design pressures are identified.

It should be noted that the paper is based primarily on experience gained on high rise buildings and may not be directly applicable either to sheds and other low rise structures or to tall masts and towers.

WIND FLOW AROUND BUILDINGS

For a general treatment of wind effects on buildings, Lawson[1] is recommended.

Fig. 1 shows typical flow patterns around three different shapes of body.

With a streamlined body the flow remains 'attached' over the whole surface and positive and negative pressures occur as shown.

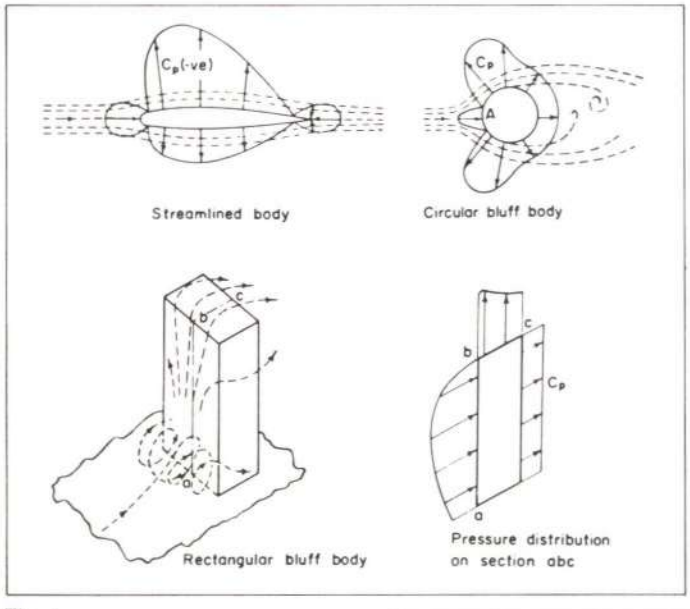

Fig. 1
Typical wind flow patterns

With the circular shape the flow is attached on the windward face but 'separates' at some point around the surface. In the attached regime both positive and negative pressures occur; in the area of separated flow the pressures are generally negative only.

The point at which the flow separates is dependent on the Reynolds Number (defined as $Re = DV/\nu$ where D is the diameter, V the velocity and ν the viscosity), the surface roughness and to a lesser extent the level of turbulence.

The wind flow around a bluff body such as a building is somewhat more complex. On the windward face, above the 'stagnation point' which is normally about $\frac{2}{3}$ of the way up, the flow turns upwards over the top of the building. Below the stagnation point the air passes downwards as shown. Towards each front edge the wind passes horizontally around the sides.

The flow is usually attached on the windward face and separated on the leeward face. On the side faces it will depend on the angle of incidence; with the wind normal to one face, the flow on both sides will be separated, although if the dimension in the direction of the wind is large the flow may 'reattach'.

With the wind on one corner the flow will generally be attached on two faces and separated on the other two.

The above comments apply mainly to smooth flow. Turbulent flow introduces fluctuations as illustrated diagrammatically in Fig. 2 and depending on the degree of turbulence, small negative gust peaks may occur on the windward face and positive peaks on the leeward face although the mean values will generally follow the above pattern.

PRESSURE COEFFICIENTS

The pressure at a point on the surface of a building subjected to wind action can be expressed as follows:

$$p = \tfrac{1}{2} \rho V^2 C_p \qquad (1)$$

where ρ is the density of air
V is the windspeed
C_p is the pressure coefficient.

The density of air in the standard atmosphere condition (101.3kPa and 15°C) is 1.225kg/m^3 and *CP3: Chapter V* is based on this.

The Australian and South African Codes are based on an ambient temperature of 20°C giving a 2% reduction in density. The density of air in the Canadian Code corresponds to a temperature of 0°C, an increase of 6% in density.

The South African Code also allows a reduction in density with altitude as follows:

Height above sea level (m)	Factor
500	0.93
1000	0.88
1500	0.83
2000	0.78

The various wind codes define how Equation (1) is to be applied although not all codes apply it in the same way. The situation is somewhat more complicated when results of wind tunnel tests are considered, as different laboratories define pressure

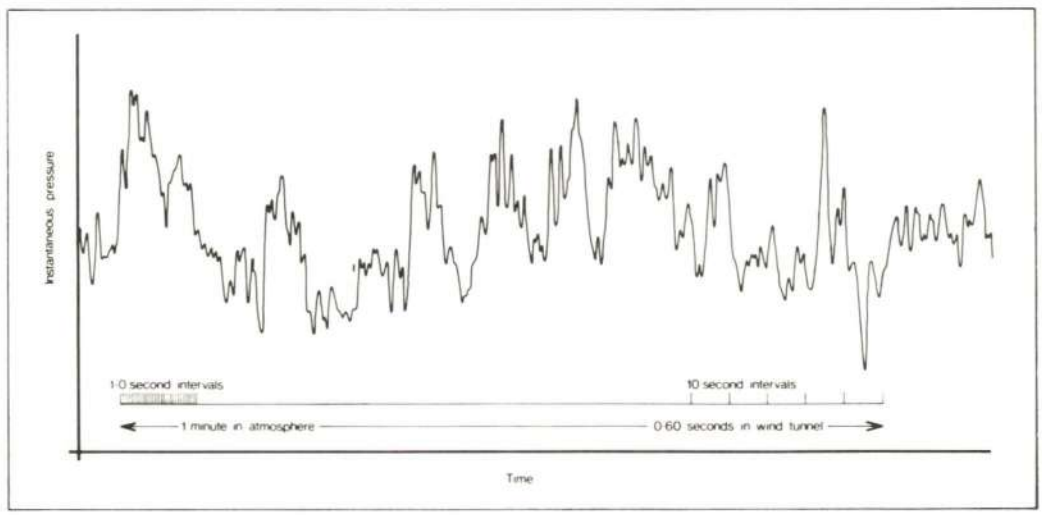

Fig. 2
Diagrammatic trace of variation of pressure with time

coefficients in different ways. For example, the windspeed can be defined as any one of the following:

(a) The mean or gust speed at the height under consideration in the free airstream upwind
(b) The mean or gust speed at the reference height (usually 10m) either at the site or reduced to a standard exposure
(c) The mean gradient windspeed
(d) The mean or gust at either the top or mid-height of the building under consideration either with or without the building there.

The pressure coefficient when applied to the mean windspeed may also either give a mean or a gust pressure, as different codes treat the effects of gusts in different ways. Considerable caution must therefore be exercised when applying Equation (1) in situations not explicitly covered by the relevant code, particularly when using information from published literature.

There is, however, a fundamental defect in Equation (1) in that it treats the pressure coefficient in a deterministic way. Although the windspeed itself is usually determined by a probabilistic approach, application of Equation (1) implies a unique relationship between velocity and pressure.

The code approach, when applicable, should be regarded as a way of achieving sensible upper bound values for strength design. However, it may bear little resemblance to what happens in reality and will usually be of limited use in serviceability calculations.

Further information on pressure distributions is available in the ESDU publications[2] although these also tend to be deterministic in approach.

If it is required to investigate pressures further, then this is best done by means of a wind tunnel test. The remainder of this paper discusses what is involved.

WIND TUNNEL TEST PROCEDURE

The first step is to make a scale model of the projected development. This need not be an exact replica of what is to be built (generally this is not possible anyway during the initial design stages when the design information is required), but should contain those elements that will have a significant effect. Some simplification is indeed of benefit when interpreting the results,as it is less likely that significant factors will be obscured by superficial effects. Similarly, the surrounding area need only be modelled in a very generalized way.

The model is then mounted in the wind tunnel on a turntable so that wind from all directions can be modelled. The size of the model is naturally limited by the dimensions of the wind tunnel as the 'blockage factor' (i.e. the ratio of the area in elevation of the model to the area of cross-section of the tunnel) must be kept sufficiently low, otherwise the edge effects of the sides of the tunnel become significant.

It is also essential that the wind structure is correctly modelled and the profiles of the variation of mean windspeed and turbulence with height should be specified. It is also necessary to specify the Power Spectral Density which defines how the turbulence is spread across the range of gust frequencies.

Further details on the procedures are contained in References 3 and 4.

STATISTICAL THEORY

Probability distributions

Fig. 3 shows three probability distributions that are commonly used in wind engineering.

It is important to distinguish between the Probability Density Function (PDF) and the Cumulative Probability Function (CPF). The CPF is the integral of the PDF.

The Normal distribution

The PDF of the Normal (or Gaussian) distribution is given by

$$p = \frac{1}{\sqrt{2\pi}} e^{-\eta^2/2} \qquad (2)$$

where $\eta = \dfrac{x - \bar{x}}{\sigma_x}$ (3)

$\bar{x}$ = the mean of x
σ_x = the standard deviation of x.

Equation (2) must be integrated numerically to obtain the CPF.

The Fisher-Tippett Type 1 distribution

Fisher and Tippett invented three distributions which they called Types 1 to 3. Gumbel was the first to apply the Type 1 distribution to naturally occurring phenomena and this distribution is therefore sometimes referred to as the Gumbel distribution.

The FT-1 distribution is commonly used in two ways in wind engineering: first to describe the occurrence of wind speeds, for example the distribution of the annual maxima; secondly, to describe the occurrence of a peak gust value, for example the maximum pressure that will occur in any one hour.

The CPF of the FT-1 distribution is given by

$$P = e^{-e^{-a(x-u)}} \qquad (4)$$

where P is the probability that x will *not* be exceeded.
u is the mode
l/a is the dispersion

It is often convenient to rearrange Equation (4) thus

$$x = u - {}^{1}/_{a} \log_e \log_e ({}^{1}/_{P}) \qquad (5)$$

When applying the FT-1 distribution it is usually convenient to work with the mode and dispersion. The mean and standard deviation, however, can be expressed as follows:

$$\bar{x} = u + \frac{0.577}{a} \qquad (6)$$

$$\sigma_x = \frac{1.282}{a} \qquad (7)$$

The Weibull distribution

While the FT-1 distribution is normally applied to the extreme values of a population, for example the maxima occurring each year, the Weibull (or Fisher-Tippett Type 3) distribution is often used to describe the population as a whole. The CPF is given by

$$P = e^{-(x/c)^k} \qquad (8)$$

Here P is the probability that x *will* be exceeded. c and k are constants.

If k = 1 then the distribution is exponential and if k = 2 it is known as the Rayleigh Distribution. Expressions for the mean and standard deviation do exist but they are in terms of gamma functions and require tables to evaluate.

Other distributions

Other distributions sometimes mentioned in the literature are the Lognormal distribution (which is a normal distribution applied to the logarithm of x) and the FT-2 (or Frechet) distribution (which is a FT-1 distribution applied to the logarithm of x).

Variation of pressure with time

The variation of pressure at a point on the surface of a building is shown diagrammatically in Fig. 2. The distribution of gust pressures about the mean value is usually well described as a

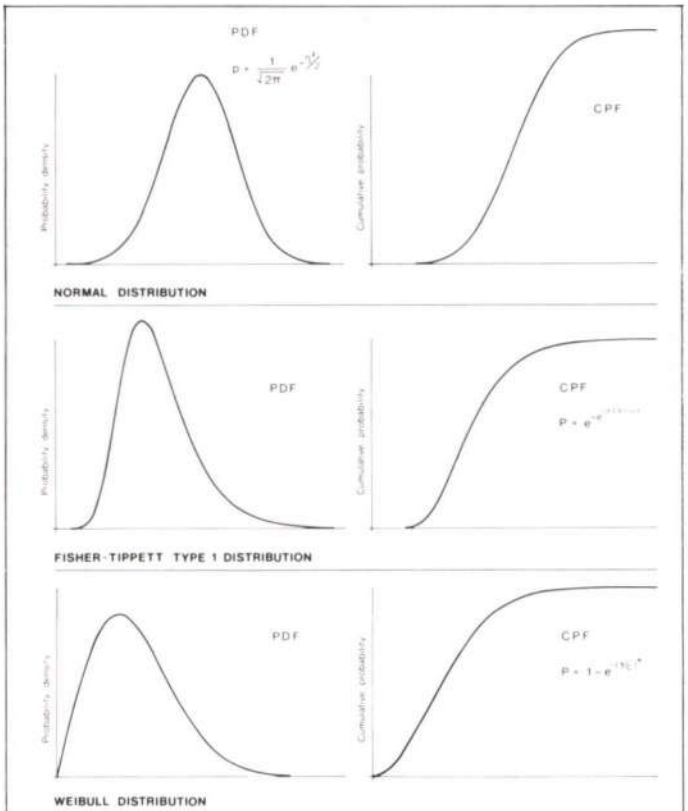

Fig. 3
Probability distributions

whole by a normal distribution (Fig. 4) (although as discussed below it does not always hold for the extreme tails).

The fluctuating pressure can be expressed in terms of a mean value (usually the mean hourly value) and the standard deviation (often referred to as the root-mean-square or RMS value). These values can be measured in a wind tunnel test.

Averaging interval

When considering the pressure on a building it is necessary to determine the appropriate averaging interval. This will depend on the size of the element under consideration, for example whether it is the whole building or a single cladding unit.

It can be seen from Fig. 4 that the shorter the averaging interval the higher the peak value will be. Only the wind eddies that are large enough to encompass the whole element or building will have an effect. Smaller eddies will not be correlated across the whole surface and will cancel each other out. The appropriate averaging interval T (in secs) is given by the following empirical relationship.

$$T = \frac{4.5L}{\bar{V}} \qquad (9)$$

where L is the representative length in metres

$\bar{V}$ is the mean hourly velocity in m/sec.

In *CP3: Chapter V* Classes A, B, and C correspond to averaging intervals of 3, 5 and 15 seconds respectively. (The 3 seconds for Class A is an historical anomaly and should be shorter. Allowance for this is made in the values of the pressure coefficients in the code.)

Extreme values

For the purpose of design we are interested in the maximum gust pressure and, having determined the mean hourly value and the standard deviation, we need to find the maximum peak value that will occur during any one hour.

One way of determining this in the wind tunnel is to run the test for one hour and measure the largest value that occurs. Unfortunately, there is a difficulty here as what may happen in one hour may not happen in another. For example one sample may contain a 'rogue' high value which might occur only once in say 100 hours. Alternatively, a high peak may not occur.

One way of overcoming this problem is to take a number of one-hour samples and then carry out an extreme value analysis to determine the expected maximum value. This, however, is expensive in tunnel time and is not normally justified.

Alternatively, the expected maximum value can be estimated by making assumptions about the statistical properties of the distribution. Fig. 5 shows diagramatically the probability distribution of all gusts and also the probabilities of the maximum pressure that will occur during a given period.

It can be shown[4] that if the parent population is normally distributed (Equations 2 & 3), then the probability of the maximum value is closely approximated by a FT-1 distribution (Equation 4) with mode and dispersion given by

$$u = \bar{x} + \sigma_x \sqrt{[2 \log_e \nu T]} \qquad (10)$$

$$a = {}^{1}/_{\sigma_x} \sqrt{[2 \log_e \nu T]} \qquad (11)$$

where ν is the cycle frequency and T is the length of time considered (ie 3600 secs).

The cycle frequency ν is given by the expression

$$\nu^2 = \frac{\int_0^\infty n^2 S_n dn}{\int_0^\infty S_n dn} \qquad (12)$$

where S_n is the Power Spectral Density at frequency n (which can be measured in the wind tunnel test) and is a measure of the distribution of different gust frequencies.

The product νT is, in effect, the number of statistically independent gusts that will occur during a period of one hour. The maximum expected value that will occur will be given by the mean of the extreme value distribution. Substituting in Equation (6) then gives

$$x_{max} = \bar{x} + \eta_1 \sigma_x \qquad (13)$$

$$\text{where } \eta_1 = \sqrt{[2 \log_e \nu T]} + \frac{0.577}{\sqrt{[2 \log_e \nu T]}} \qquad (14)$$

As already noted, however, in areas of separated flow the assumption of the normal distribution does not hold for the extreme tails of the distribution and Lawson[1] suggests an exponential relationship (above $\eta = 2.7$) of the form

$$p = \frac{1}{\sqrt{2\pi}} e^{-1.35\eta} \qquad (15)$$

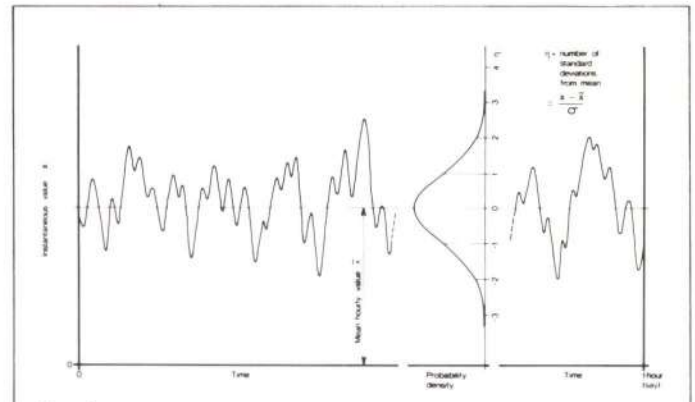

Fig. 4
PDF of fluctuating pressure

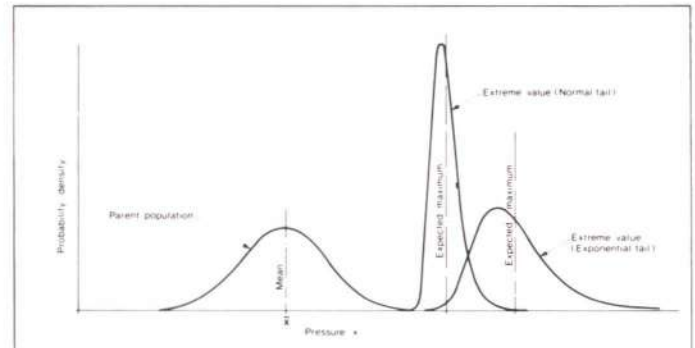

Fig. 5
PDF's of parent and extreme pressures

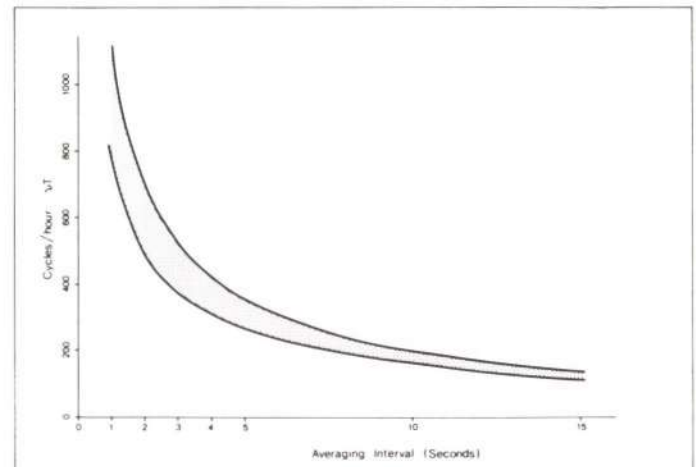

Fig. 6
Variation of νT with averaging interval

It can be shown[4] that, for the exponential tail, Equation (13) also holds but with Equation (14) replaced by

$$\eta_2 = (\log_e \nu T + 0.577)/1.35 \qquad (16)$$

In order to determine these values it is necessary first to evaluate νT. Published data seems to indicate that νT normally lies in the range 100-1000 but more detailed information on the subject is scarce. For the present purpose it has been evaluated by applying Equation (12) to the ESDU formula[2] for the Power Spectral Density for the free air flow but truncated at the frequency corresponding to the averaging interval. The results are shown in Fig. 6.

Typical values for η_1 and η_2, obtained in this way, are shown in Table 1.

Table 1

Averaging Interval (t secs)	νT	η_1	η_2
0.5	1400	3.95	5.78
1	950	3.86	5.51
3	450	3.66	4.95
5	300	3.55	4.65
10	180	3.40	4.27
15	130	3.31	4.03
30	70	3.11	3.57
60	35	2.87	3.04

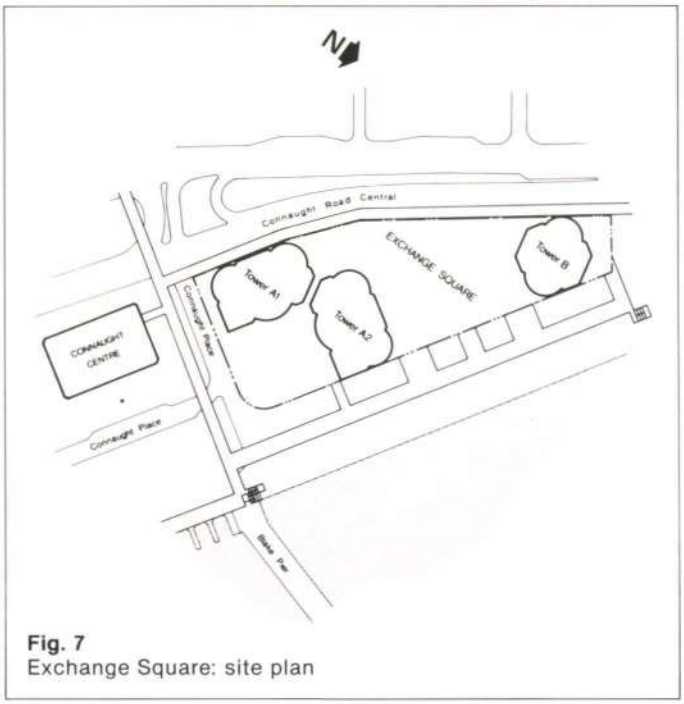

Fig. 7
Exchange Square: site plan

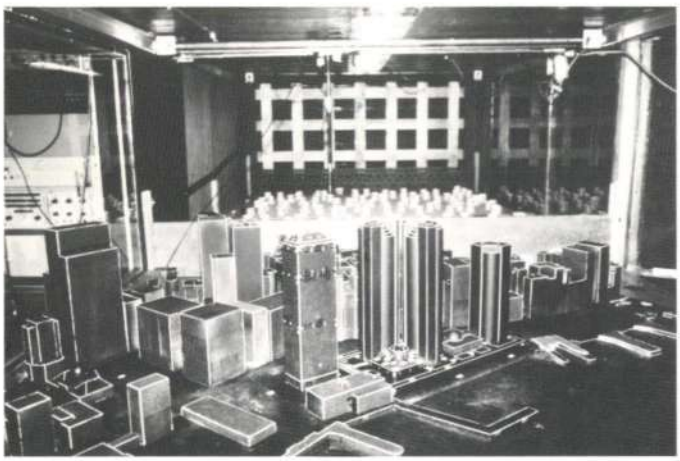

Fig. 8
Exchange Square: wind tunnel model

CASE STUDY: EXCHANGE SQUARE, HONG KONG

Project description

The site for the Exchange Square Development is located in central Hong Kong close to the Star Ferry terminal and the existing Connaught Tower (Fig. 7).

The development comprises two 50-storey and one 37-storey office towers above an open plaza at first floor level. Beneath the plaza are the bus stations for The China Motor Bus Company and the Public Light Bus Company. Also included in the development is a new Stock Exchange trading hall.

Test details

Wind tunnel tests were carried out by the Department of Aeronautical Engineering at Bristol University during the period September-November 1982. These tests included pressure measurements on the two 50-storey towers and around the base and also on the Connaught Tower. An environmental wind test was also carried out.

The model (Fig. 8) was made to a scale of 1:500. The details of the surrounding buildings were based on photogrammetric readings taken from aerial photographs supplemented by additional information on nearby buildings under construction. The total numbers of pressure tapping points were 297 on Exchange Square and 180 on Connaught Centre. The time scale was 1:100.

The wind simulation was based on the work carried out at the Boundary Layer Wind Tunnel Laboratory, Ontario, Canada (BLWTL) in connection with the Hongkong and Shanghai Bank. The results of those studies indicated that the wind profiles from all directions can be modelled with five alternative exposures as shown in Fig. 9.

Pressures at each tapping point were measured for wind directions at 15° intervals. For some directions two or more exposures were specified and the worst case taken so that there were a total number of 33 permutations of direction and exposure.

Further details are given in reference (4).

Results

Contours of peak positive and negative one-second gust pressures for the two towers A1 and A2 are shown in Fig. 10. These results all correspond to the 50-year wind (mean hourly gradient velocity 47.1 m/s) acting in the worst direction for each location. Polar plots showing the variation of pressure with wind direction at four critical locations are shown in Fig. 11.

The maximum negative one-second gust pressure occurred at location 15 which is at the top level on the north cylinder on Tower A2. The reason for this is the curved surface to which the flow sticks rather than separating at a sharp edge and this in turn induces a higher surface speed and hence a higher suction.

High suctions also occurred at Locations 38 and 60 which were directly below Location 15. It is interesting to note that the

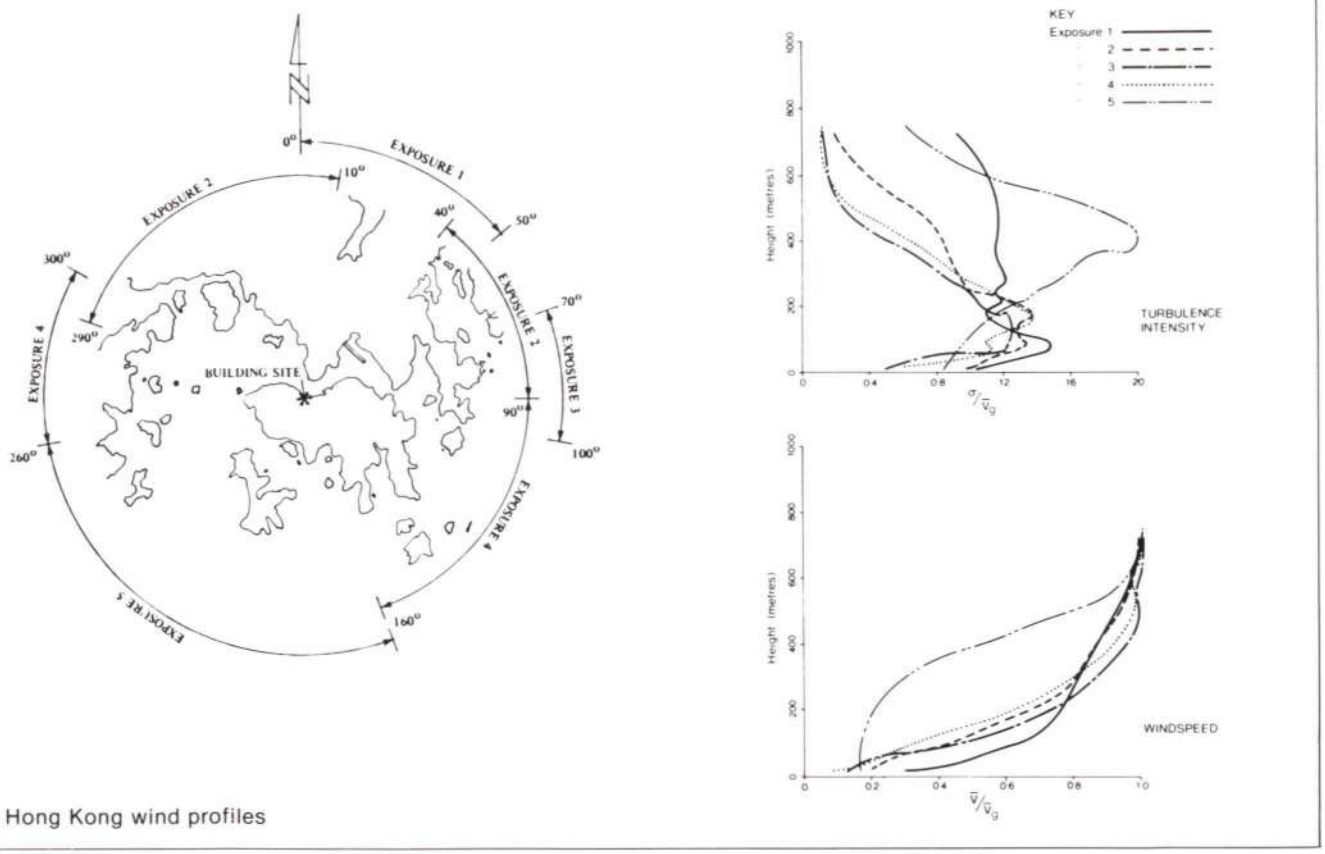

Fig. 9
Central Hong Kong wind profiles

maximum one-minute suction occurred at Location 60 and the maximum mean suction at Location 38, indicating that the general flow pattern is similar for most of the height. The mean pressure was a maximum near midheight while the turbulence increased both above and below that level.

This band of high suction was quite narrow in both size and wind direction as demonstrated by Figs. 10 and 11.

The same effect did not occur at the corresponding position on Tower A1. This was because of the shielding by the Connaught Tower for the critical wind direction.

There was an interesting high suction at location 160 near the base of the south-east facade of Tower A1. This was probably due to the proximity of the Connaught Tower causing a 'Venturi' effect in the gap between. The fact that it occurred near ground level may be due to the speed-up of the wind and separation from the roof of the trading hall at the base of the towers.

In comparison, the pressures in the gap between the Tower A1 and A2 were very much a non-event, indicating that this gap is sufficiently small to make the wind pass round the outsides of the two towers rather than in-between.

The maximum positive gust pressure occurred at location 166 near the base of Tower A1.

EFFECT OF WIND CLIMATE

General

The results presented above are for the situation of the 50-year wind (from all directions combined) acting in the worst direction for each location.

These values are compatible with the definition of characteristic or working wind loads implied by *CP3:Chapter V* when used in conjunction with *CP110, CP114* or *BS449*. They will, however, overestimate, often quite significantly, the values that will occur at each location once in 50 years. For example, if the maximum pressure occurs over only a small range of wind directions (Fig. 11) and if the latter coincide with those from which strong winds do not occur, then the probability of a high pressure occuring at that location will be greatly reduced.

Hong Kong wind climate

The results of the BLWTL Hong Kong Climate study indicated that the high wind speeds appropriate to strength design are invariably associated with typhoons. The results of the BLWTL typhoon model can be fitted by a Weibull function (see above) thus

$$N = Ae^{-\left(\frac{V}{C}\right)^k} \qquad (17)$$

where N is the number of hours/year on average that V is exceeded.

V is the gradient mean hourly velocity.

A, C and k are constants for each wind direction and are available tabulated for 15° azimuth intervals. Equation (17) is shown plotted in Fig. 12.

Integration by azimuth

From Equation (17) and assuming that the pressure at each point is proportional to the square of the gradient velocity, the number of hours/year N_x that a pressure X is exceeded is given by

$$N_x = \sum_{\theta=0}^{360} A_\theta e^{-\left(\frac{\bar{V}_{50}}{C_\theta}\sqrt{\frac{X}{X_{50,\theta}}}\right)^{k_\theta}} \qquad (18)$$

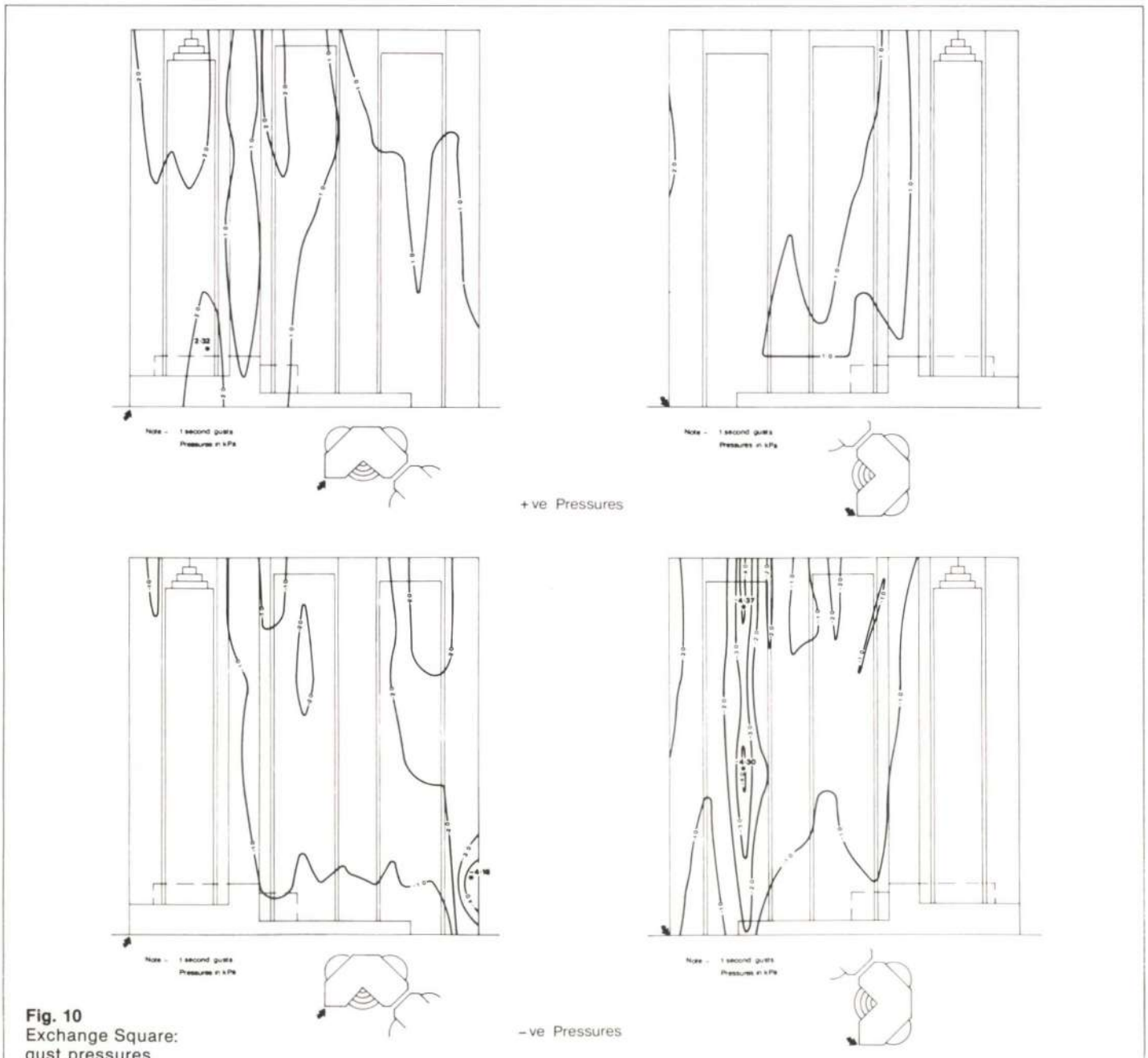

Fig. 10
Exchange Square: gust pressures

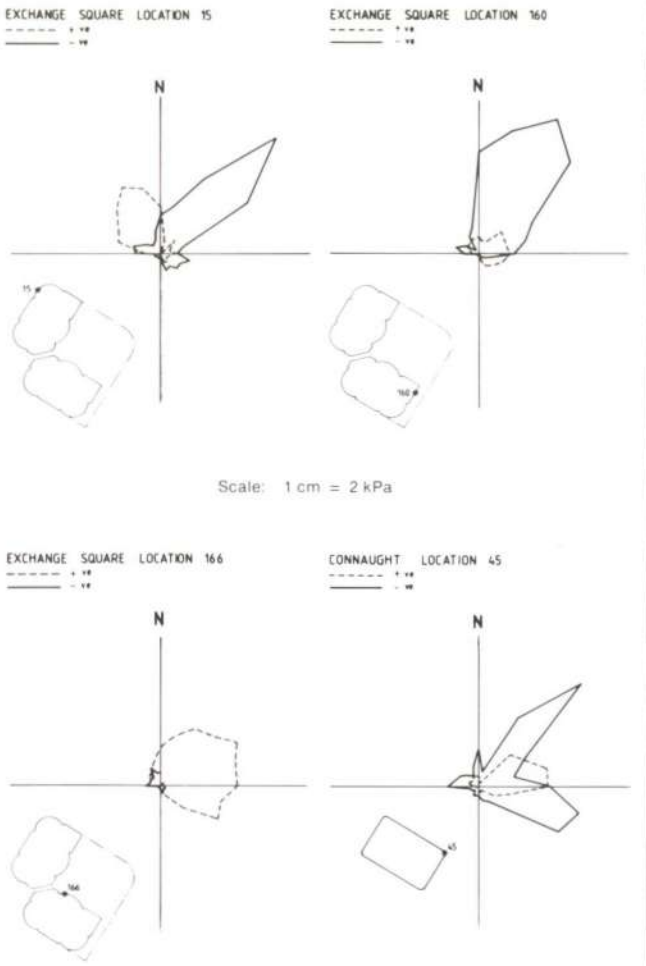

Fig. 11
Variation of pressure with wind direction

where $\bar{V}_{50}$ is the 50 year gradient velocity (47.1 m/s)
$X_{50,\theta}$ is the pressure at the point with $\bar{V}_{50}$ at θ
A_θ, C_θ and k_θ are the Weibull coefficients for angle θ.

Equation (18) gives the number of hours *on average* that a given value X will be exceeded. If each hour of wind was statistically independent then the return period R (in years) for a given value of X would be given by $R = 1/N_x$. Successive hours of wind however, are not independent and one typhoon will produce several hours of high winds. It can be shown[5] that, for the Hong Kong typhoon climate as given by Equation (17), the return period R of X occurring is given by

$$R = \frac{14.8}{N_X} \qquad (19)$$

Equation (19) implies that in a typhoon there are, on average, 14.8 statistically dependent hours of wind.

The above approach is greatly simplified and a more rigorous treatment as used at BLWTL is presented by Surry *et al*[6]. Results from the above method, however, have been compared with those obtained by BLWTL and agreement generally found to be within 2%.

The results for some of the critical locations on Exchange Square are shown plotted in Fig. 13 and the 50 year event values are shown plotted against the values with the 50 year wind in the worst direction in Fig. 14.

Expected maximum values

Having found values of the pressure X for various return periods (R), we can now consider the maximum value that can be expected to occur within a given lifetime.

It is evident from Fig. 13 that the pressure X is effectively a linear function of log R, i.e.

$$X = X_{50} + {}^{1}/_{a} \log_e (R/50) \qquad (20)$$

where X_{50} is the 50-year return period value and a is a constant from which

$$N = {}^{1}/_{R} = {}^{1}/_{50}\, e^{-a(X - X_{50})} \qquad (21)$$

where N is the average number of occasions per year that X will be exceeded. (N here is the number of statistically independent events and should not be confused with N_x which is the total number of events per year.)

The expected number of such occurrences in T years is thus NT. Assuming a Poisson distribution for the arrivals, then the probability P_T of X not being exceeded in T years is given by

$$P_T = e^{-NT} = e^{-T/50\, e^{-a(X - X_{50})}} \qquad (22)$$

which, for a design lifetime of 50 years, reduces to

$$P_{50} = e^{-e^{-a(X - X_{50})}} \qquad (23)$$

Equation (23) will be recognized as an FT-1 distribution, Equation (4). The expected maximum value $\bar{X}$ that will occur during the design lifetime will be the mean of this distribution which, from Equation (6) is given by

$$\bar{X} = X_{50} + \frac{0.577}{a} \qquad (24)$$

The value of a can be found conveniently from Equation (20) thus

$${}^{1}/_{a} = (X_{100} - X_{50}) / \log_e 2$$

$$\therefore \bar{X} = 0.168 X_{50} + 0.832 X_{100} \qquad (25)$$

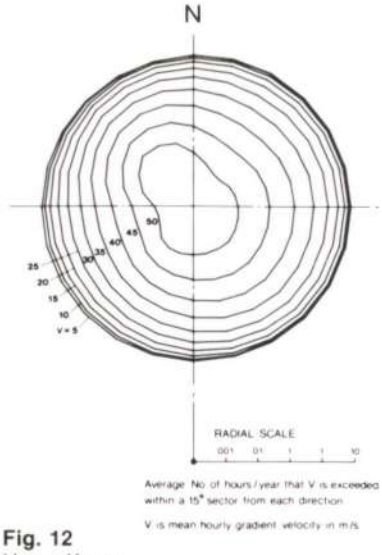

Fig. 12
Hong Kong typhoon climate

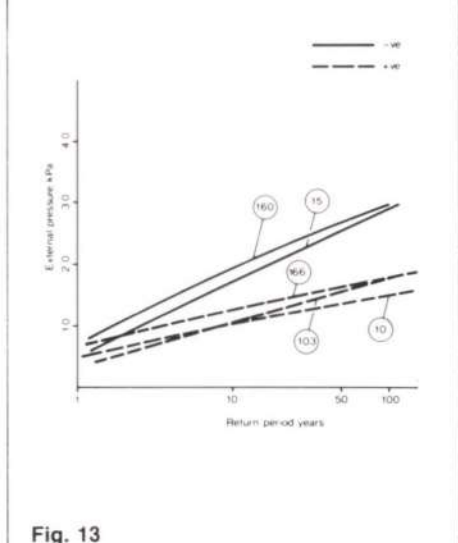

Fig. 13
Extreme pressures at selected locations

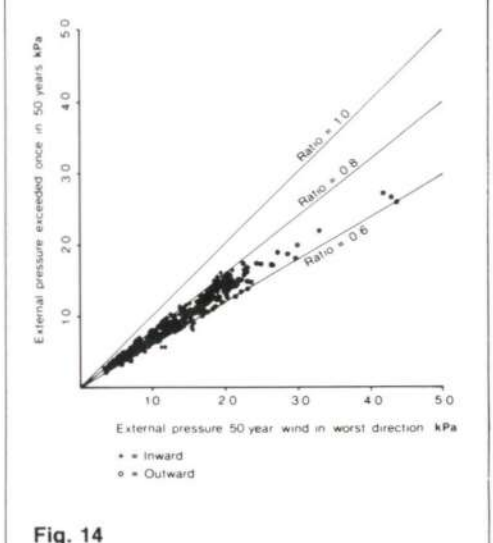

Fig. 14
External pressures: 50 year values

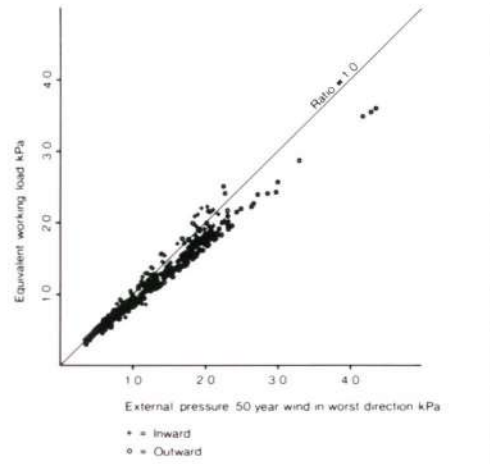

Fig. 15
External pressures:
equivalent working loads

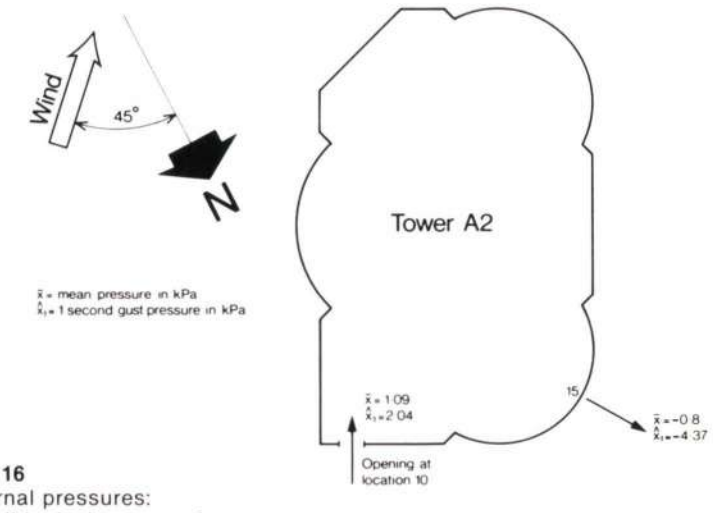

Fig. 16
Internal pressures:
possible design scenario

Allowance for uncertainty

The conventional definition of the characteristic wind load as noted above is that load which occurs with the 50-year wind acting in the worst direction for the member under consideration. It is evident that this will always be an upper bound to the load which will occur once in 50 years. (The two values would be the same if the pressure coefficient at the point was the same for all wind directions, for example, at the top of a circular dome.) It follows that although the characteristic value of the pressure, if defined in this way, is not a very good estimate, it will tend to be on the safe side and the probability that it will be exceeded will be correspondingly reduced.

In contrast, the expected maximum value during a specified design lifetime as derived above will, by definition, be a better prediction. It will, in fact, have roughly a 50% probability of being exceeded (the expected value is taken here as the mean of the extreme value distribution and the mean and the median are not very different). This logically requires a larger factor of safety to be applied in the design.

In order to determine an appropriate load factor to use in this case the method contained in the draft Part 2 of the revised *CP110* and described in more detail in reference (7) has been used. The basis of that method is that the required ultimate structural resistance R_u is related to the expected maximum load effect $\bar{S}$ as follows:

$$R_u \geqslant 0.94\bar{S}\,(1 + 4.8\sqrt{(0.01 + 0.77v^2)}) \qquad (26)$$

where v is the coefficient of variation of S.

In this case the expected value is given by Equation (24) and all that is required is to find an appropriate value for v.

The uncertainty is made up of two parts:

(a) The possibility of an extreme wind occurring in a critical direction assuming that the statistical analysis is correct: i.e. the variability of the wind climate itself.
(b) The uncertainties in the statistical analysis, the wind simulation and the pressure readings, i.e. the uncertainty in our understanding of the wind climate.

The effects of (a) can be determined from the properties of the FT-1 distribution for which the standard deviation is given by Equation (7).

For (b) a value of 10% has been taken:

Combining the uncertainties

$$v^2 \doteqdot \left(\frac{1.282}{a\bar{x}}\right)^2 + 0.1^2 \qquad (27)$$

In order to compare this approach with the traditional definition of the characteristic value, the results from Equation (26) have been divided by a load factor of 1.6 to produce equivalent working loads and these are shown plotted in Fig. 15.

The results, in this case, show that the traditional definition is generally quite adequate for the bulk of the results. However, it overestimates the higher suctions, where the effects described above will be most pronounced, by up to 20%.

INTERNAL PRESSURES

General

In addition to the external pressures as measured in the wind tunnel test, allowance must be made for the internal pressures within the building.

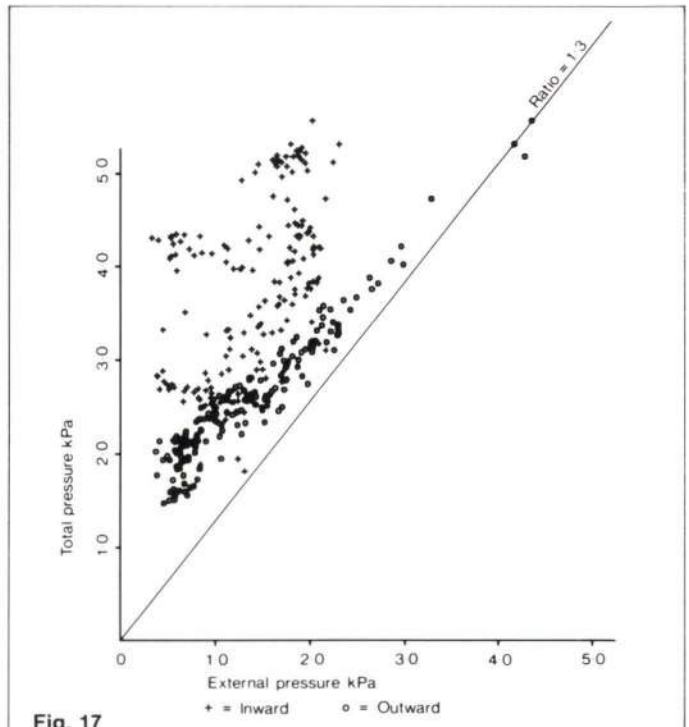

Fig. 17
Total pressures v. external pressures

For the case of full air-conditioning and cladding which is nominally airtight, the permeability of the outer skin of the building, under normal conditions, will be very low. The internal pressure will therefore be largely governed by the disposition of the A/C intake and exhaust, the effect of which is difficult to quantify, even when this information is available.

CP3 Chapter V suggests, in such cases when there is a 'negligible probability' of a dominant opening occurring, pressure coefficients of +0.2/-0.3, whichever is more onerous. Comparing these with the maximum relevant coefficients for the external pressures in the same code (−1.2/+0.8) indicates an extra 17% or 38% on negative and positive external pressures respectively.

Guidance on internal pressures is also given by the Canadian Wind Code, which for this case indicates pressures of the order of ± 0.5 kPa for the case without dominant openings.

The HK Wind Code requires a value of +0.6P/−0.5P (where P is the basic pressure) for nominally airtight surfaces and ±0.9P for surfaces which are openable or breakable.

If dominant openings can occur (in this context a single broken window could be considered as a dominant opening) then the Canadian code suggests applying a gust factor of 2.5 to the figures quoted above i.e. ± 1.25 kPa.

The UK code for this condition gives various values for pressure coefficients depending on where the opening occurs, up to a maximum of +0.6/−0.9 leading to extra pressures of 50% and 110% respectively.

Two design cases can thus be identified: first the normal situation in which the outer skin of the building remains intact, the second when a dominant opening occurs.

The effect of an opening occurring in a critical position has been studied using the Exchange Square test results by sub-dividing them into groups in each tower and at the same level. For each location and for each wind direction the effect of an opening occurring at each other location at the same level is considered and the worst case found.

First, however, it is necessary to determine the relationship between the pressure inside and the pressure immediately outside an opening. This will depend on how quickly the internal pressure can follow the change in pressure outside. This is examined in detail in Reference (5) where it is shown that the time t in seconds to reach equilibrium is given by

$$t = 2.5 \times 10^{-4} (V/A) \sqrt{\Delta p} \qquad (28)$$

where V is the volume (m^3), in this case of one floor of the building.

A is the area (m^2) of the opening.

Δp is the initial pressure difference between inside and outside (Pa).

Taking $V = 4000\ m^3$, $A = 2m^2$ and considering, for example, location 15 wind direction 45°, the time taken for the internal pressure to change from the mean value (800Pa) to the maximum negative value (4370 Pa) will be

$$t = 2.5 \times 10^{-4} \times \frac{4000}{2} \sqrt{3570} = 3 \text{ secs.}$$

If, however, the floor is subdivided by partitions the volume will be decreased and hence the time taken to reach equilbrum could be somewhat less.

The conservative assumption can therefore be made that the internal pressures will be equal to the one-second external pressures immediately outside an opening.

Having determined the internal pressure it is necessary to decide how it will combine with the external pressure at another location. This will depend on whether or not the pressures are correlated. In this case it seems reasonable to assume zero correlation and the total pressure p can then be estimated from

$$p = \bar{p}_e + \bar{p}_i + \sqrt{|(\hat{p}_e - \bar{p}_e)^2 + (\hat{p}_i - \bar{p}_i)^2|} \qquad (29)$$

where $\bar{p}_e$ $\hat{p}_e$ are the external mean and gust values

$\bar{p}_i$ $\hat{p}_i$ are the internal mean and gust values.

The maximum resultant pressure obtained in this way occurs again at location 15 with an opening at location 10 as illustrated in Fig. 16. The maximum outward one-second pressure is given by

$$p = 0.8 + 1.09 + \sqrt{|(4.37 - 0.8)^2 + (2.04 - 1.09)^2|}$$
$$= 5.58 \text{ kPa}$$

This represents an increase of 28% on the external pressure, which by coincidence agrees well with the value of 30% suggested by the American cladding consultant on the project as being common practice in the USA.

There is a corollary, however, to this calculation. If an opening occurs at location 15 then, for the same wind direction (45°), the resultant inward pressure at location 10 will also be 5.58 kPa, an increase of 170% on the external pressure.

Common sense, however, suggests that if location 15 is designed for a greater pressure than location 10 then the probability of an opening at location 15 will be less than that at 10 and therefore the design pressure at the latter should be lower. The relationship between strength required to that provided clearly affects the probabilities in a way that is difficult to quantify.

In Fig. 17 total pressures at each point are plotted against external pressures. It will be seen that in virtually all cases the ratio exceeds the suggested value of 1.3. The effect is more pronounced for inward pressures and it is apparent that a critical condition will, in theory, arise if an opening occurs at a point of high suction. It should, however, be noted that breakage is itself an unlikely event and if account could be taken of this probability the design values would be correspondingly reduced. Unfortunately, this is not readily quantifiable.

The conclusions that can be drawn from this are, to a certain extent, philosophical. On the one hand it can be argued that the design pressure at any one level should be the same and this is compatible with the benefits of maintaining uniformity of strength and detail. Alternatively, it can be argued that the best protection is to strengthen these critical areas and hence reduce the possibility of breakage occurring there. Furthermore, should a breakage occur then it could be regarded as an extreme case in which a reduced factor of safety would be justified.

However, as discussed in the next section, internal pressures are not the only difficulty.

DESIGN VALUES

The various factors that can logically be considered in determining design pressure include the following:

(1) Variation of pressure at each location with wind direction
(2) Variation of probability of wind speeds occurring with wind direction
(3) Internal pressures and design scenarios
(4) Possibility of knock-on effects, i.e. damage to other panels caused by the failure of one panel
(5) The variability of cladding strength including time-dependency
(6) The design life of the cladding
(7) Acceptance criteria. Assuming some failures (e.g. broken windows) during the design lifetime are acceptable, how many, how often? What level of safety is required?
(8) Statutory requirements
(9) Other factors besides strength will often govern the design, e.g. uniformity of glass thickness, colour and flatness, repetition of details, light and heat transmission, durability, etc.
(10) Contractual matters including the specification, design responsibilities and guarantees, load test requirements etc.

Of this list Items 1-3 have been discussed in the sections on wind climate and internal pressures above. Item 4 is not readily quantifiable and items 8-10 are beyond the scope of this paper.

Under Item 5 it is worth noting that when considering the strength of glass, the appropriate averaging interval may well be of a longer duration because of the reduction in strength with duration of load. For example, the ratio of the one-second strength to the one-minute strength may well be greater than the ratio of one-second to one-minute pressures.

Items 6 and 7 can, in theory at least, be decided by the designer although designers are notoriously (and justifiably) coy about defining design lifetimes for their buildings. (Incidentally, it is worth noting that if a building has 500 windows each exactly designed for the 50-year event, it does not follow, as is sometimes suggested, that 10 windows will break each year. The loads on individual elements are not statistically independent events.)

CONCLUSIONS

A number of conclusions can be summarized as follows:

(1) The decision to embark on a wind tunnel test is not one that should be taken lightly. Although such tests will usually give a better qualitative understanding of the effects of wind on the building, clients and architects normally expect more tangible benefits. If the results are to be used quantitatively, great care must be taken when specifying the test and in interpreting the results as the latter will, to a large extent, reflect the various assumptions made.

(2) The wind tunnel path leads immediately away from the cosy world of deterministic pressure coefficients and the designer must be prepared to accept that the results will be in the form of probabilistic statements which may not readily be assimilated into the design process. In particular it requires acceptance criteria that are also probabilistic in form.

(3) In some case more benefit will be achieved at less expense and in a shorter time by a study of the local climate and the effects of local topology than by carrying out a wind tunnel test.

(4) If information is available on the directional probabilities of the wind climate then lower design pressures can be obtained by integrating the wind tunnel results with the wind climate. However, if this is done then caution must be exercised as conventional load factors may not be appropriate to the resulting pressures.

(5) Internal pressures are difficult to deal with in a logical manner and the question of the appropriate design scenario requires resolution.

References

(1) LAWSON, T.V. Wind effects on buildings: Volume 1: Design applications. App Science Publishers, 1980.

(2) ENGINEERING SCIENCE DATA UNIT (ESDU). Various data items. (Sets of these are held by David Croft and John Tyrrell).

(3) CROFT, D.D. Tsuen Wan wind tunnel tests, *The Arup Journal, 14* (4), pp. 14-18, 1979.

(4) OVE ARUP PARTNERSHIP Job 11575/52: Exchange Square wind tunnel test, Report No. 3, Feb 1983.

(5) *Ibid*, Report No. 4, Feb 1983.

(6) SURRY, D. *et al.* Wind induced exterior suctions and pressures on the new Hongkong and Shanghai Bank Building, Hong Kong. Univ. of Western Ontario. Eng. Science Research Report, BLWT-SS14-1981 (Prelim).

(7) CROFT D.D. An alternative approach to ultimate limit state design, *The Arup Journal, 17* (2), pp. 13-18, 1982.

Structural response

Michael Willford

SYNOPSIS

The trend in building design towards taller, lighter and more flexible forms has led to buildings that can be susceptible to significant dynamic wind responses. The responses that are of primary concern are

(a) Peak structural loads (enhanced by dynamic magnification)

(b) Peak sway deflections (enhanced by dynamic magnification)

(c) Fatigue cycling

(d) Movements that are perceptible to occupants.

Traditional quasi-static methods cannot adequately predict the behaviour of dynamically sensitive structures.

The aim of this paper is to outline the basic principles involved and to describe some of the methods that are currently available as design tools. It is seen that the prediction procedure is a three-part process:

(1) Determine the properties of the wind at the site

(2) Determine the overall aerodynamic forces on the building including the spectrum of the fluctuating components

(3) Determine the dynamic response of the building to these forces.

WIND FORCES ON BUILDINGS

Wind flow around buildings is described in Section 2 of David Croft's paper on surface pressures, and in more detail by Lawson[1].

A building standing in a flow of turbulent wind will be subjected to randomly fluctuating aerodynamic forces in the along-wind (drag), cross-wind (lift) and torsional directions as illustrated in Fig. 1. All these forces will depend on the direction, velocity profile and turbulence characteristics of the incident wind, and also on the shape of the building. Although analytical methods exist to predict the along-wind forces (provided the wind characteristics and drag coefficient of the building, including any variation with height, are known) in general, model testing techniques are required to obtain full information. Rigid models mounted on base balances may be used for this purpose with the following qualifications:

(i) Reynold's number effects

One of the compromises invariably required in the wind tunnel modelling of structures in simulated boundary layer flows is a mismatch of Reynold's number. This is not important when dealing with sharp-edged structures (e.g. rectangular buildings) because the flow separation points are defined by the geometry of the structure. However for more streamlined bodies, such as cylindrical chimneys, the separation points are related to Reynold's number and it is not normally possible to obtain realistic results from a small-scale test.

(ii) Aeroelastic effects

Aeroelasticity is the phenomenon of the interaction of aerodynamic forces and structural movements. This can lead to aerodynamic instability where successive oscillations of a structure affect the aerodynamic forces in such a way as to further excite the oscillation. This is a problem that can be encountered in slender chimneys and long-span suspension bridge decks for example. It is not normally a consideration in buildings.

In the absence of aeroelastic effects the total response of a building can be calculated using aerodynamic forces measured on rigid models (or estimated analytically) and the structural dynamic properties of the building, as will be illustrated later. In this calculation aerodynamic forces are required in mean and fluctuating components, not simply peak values. Fluctuating components are expressed as rms values (giving the total magnitude of fluctuations) and the power spectral density (giving the frequency distribution of fluctuations).

The effects of wind gusts on the drag force are now discussed for a building with a nominal size B and drag coefficient C_D.

If the instantaneous total wind speed is $V = \bar{V} + v$

where $\bar{V}$ = mean hourly
and v = gust speed

then total instantaneous drag force is

$$F_D = \tfrac{1}{2}\rho V^2 B^2 C_D$$

$$= \tfrac{1}{2}\rho B^2 C_D(\bar{V}^2 + 2\bar{V}v) \quad \text{ignoring second order terms}$$

$$= F_D\left(1 + \frac{2v}{\bar{V}}\right) \quad \text{where } F_D \text{ is the mean drag force}$$

It can be seen that the fluctuations in F_D are expected to be proportional to the fluctuations in v. In practice this is not the case over the full frequency range of gusts for the following reasons:

(i) Drag coefficient C_D is observed to vary somewhat with gust frequency.

(ii) Lack of correlation of small gusts (i.e. smaller in scale than the building size) over the building surface causes a reduction of drag force fluctuations at higher frequencies. This is known as the aerodynamic admittance effect, and its modification to the effective drag coefficient is illustrated in Fig. 2.

STRUCTURAL DYNAMICS

A brief discussion of the principles and terminology of structural dynamics is given below, as a necessary preliminary to the description of response to fluctuating wind forces.

Simple one-degree of freedom structure

Reference is first made to a very simple structure illustrated in Fig. 3, consisting of a mass M at the top of a light vertical elastic cantilever. The lateral stiffness of the tip of the cantilever is K (i.e. its lateral deflection under static lateral load P is P/K). If the mass is displaced laterally and then released, the system will oscillate from side to side with frequency n_o where

$$n_o = \frac{1}{2\pi}\sqrt{K/M} \quad \text{(Hz)}$$

This is the natural frequency of the structure. The deflected shape of the structure when vibrating in a single mode is referred to as the modeshape.

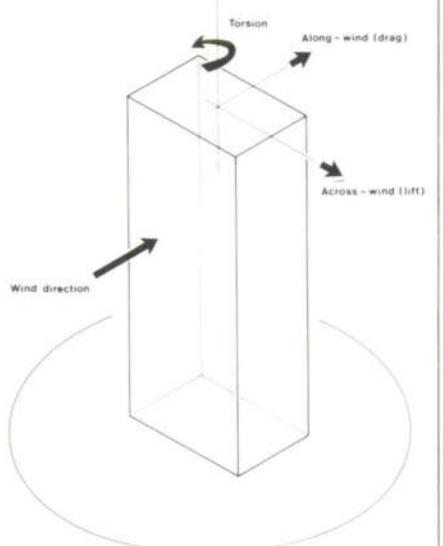

Fig. 1
Wind-response directions

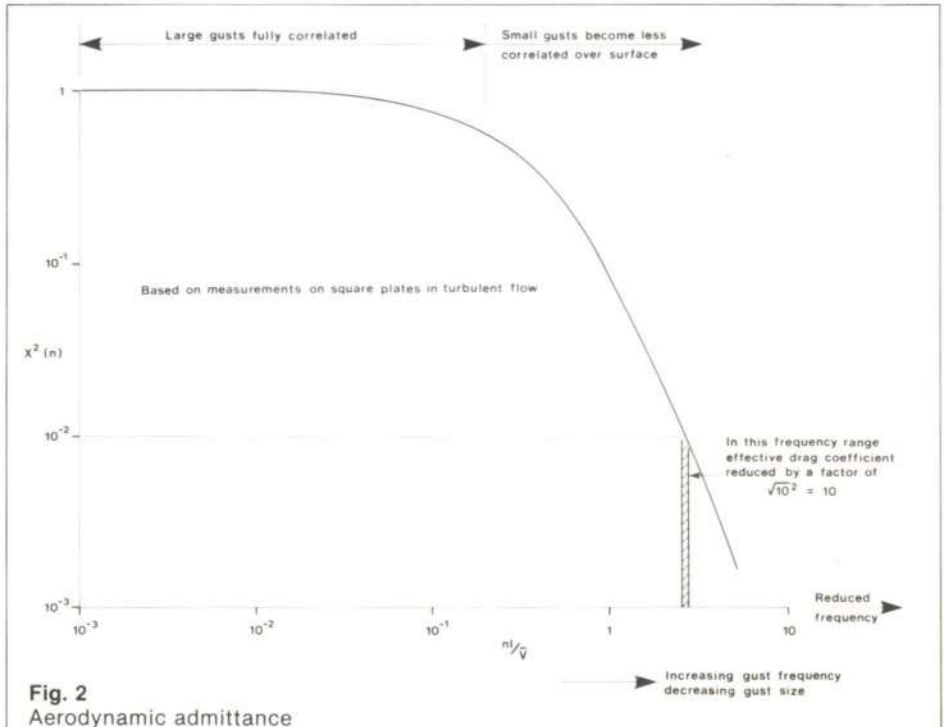

Fig. 2
Aerodynamic admittance

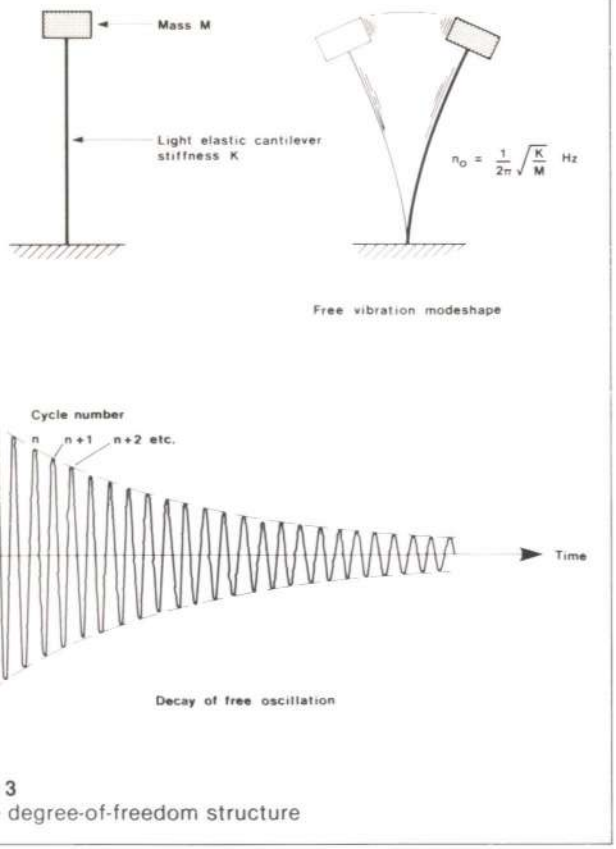

Fig. 3
One degree-of-freedom structure

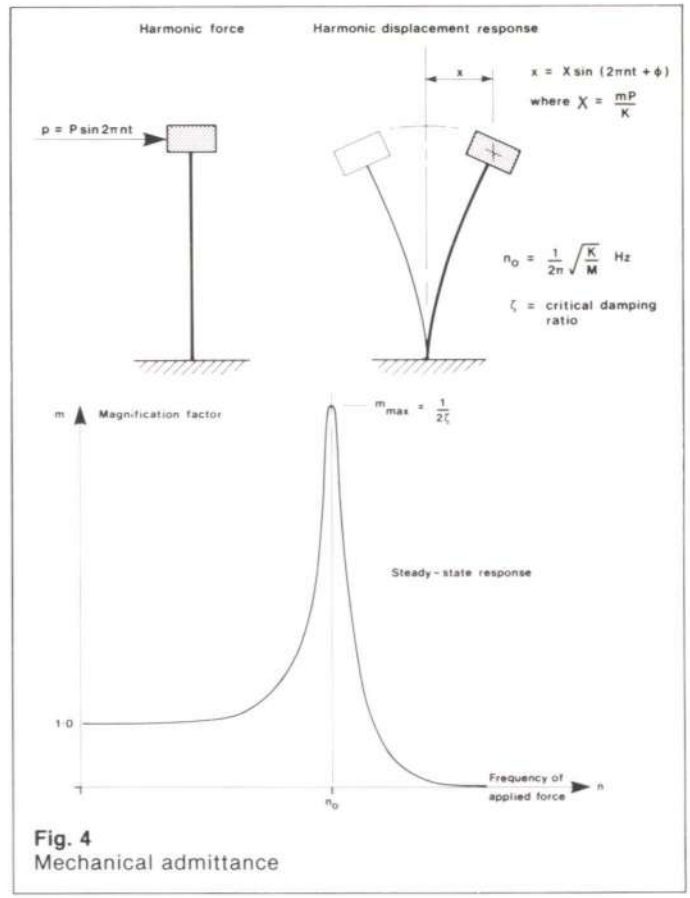

Fig. 4
Mechanical admittance

If the structure is left to oscillate the amplitude of its motion will gradually decay as energy is dissipated in damping. Damping is usually expressed as ζ which is the proportion of the critical damping of the structure (critical damping is the minimum damping necessary to cause the structure to move in one direction to rest after being released, with no oscillation). Practical structures are lightly damped with typically 0.5% to 2% of critical damping. Structural damping can be estimated from the decay rate of free oscillation as follows:

The logarithmic decrement δ is defined as

$$\delta = \log_e\left(\frac{\text{amplitude in cycle N}}{\text{amplitude in cycle N + 1}}\right)$$

and $\quad \zeta = \delta / 2\pi$

If the structure is now subjected to a harmonic force $p = P\sin 2\pi nt$ applied to the mass, its response will vary with the frequency of the force, n, as illustrated in Fig. 4.

For frequencies well below the natural frequency of the structure the response is quasi-static, the instantaneous force and deflection being

$$p = P\sin 2\pi nt$$
$$x = X\sin 2\pi nt \quad \text{where } X = P/K$$

As n approaches n_o a resonance occurs causing dynamic magnification of the response amplitude. When a steady state has been reached:

$$X = mP/K$$

where $m_{max} = \frac{1}{2\zeta}$ at $n \triangleq n_o$

For lightly damped structures this resonance occurs over a narrow band of frequencies with a high resonance magnification factor. Note that as the damping ratio tends to zero the magnification tends to infinity. The steady state response takes some time to build up. A fraction R of the steady state response will be achieved after N cycles of steady excitation where

$$N = \frac{-\log_e(1-R)}{2\pi\zeta}$$

As the applied frequency is increased beyond n_o the response amplitude decreases rapidly. The inertia of the system increases its apparent stiffness to rapidly alternating forces.

The variation of response with frequency illustrated in Fig. 4 is known as the mechanical admittance of the system. As indicated above, wind-induced forces contain a wide spectrum of frequencies. The mechanical admittance is a 'transfer function' by which the response spectrum can be obtained from the aerodynamic force spectrum. This procedure is described below in the section on calculation of responses.

Practical building structures

The dynamic properties of practical building structures lead to the same general characteristics as those described above. However, the precise formulation is more complex because

(a) Mass, stiffness and loading are continuously distributed, not conveniently separated and localized.

(b) Buildings are three-dimensional.

The continuous distribution of mass and stiffness means that many modes of vibration are possible, each with its own natural frequency. A family of lateral modeshapes for one principal direction of a uniform tall building is shown in Fig. 5 in order of increasing natural frequency. A second family of similar mode shapes will be present for a second principal translational direction, and third family for torsional modes. In other words for a practical 3-D structure there are three 'first modes', three 'second modes', etc., where 'first' and 'second' describe the general elevational shape of the mode.

If the mass and stiffness centres do not coincide in plan throughout the structure the modes will not be simple translational and torsional modes. There will still be three 'first modes' but each may contain a mixture of translation and torsion. This is illustrated by Figs. 10 to 12 showing the arrangement and modeshapes of the Hongkong and Shanghai Bank Building.

In practice it is found that generally only the first modes make any significant contribution to wind-induced response of tall buildings. Second modes may however become significant near the top of a building.

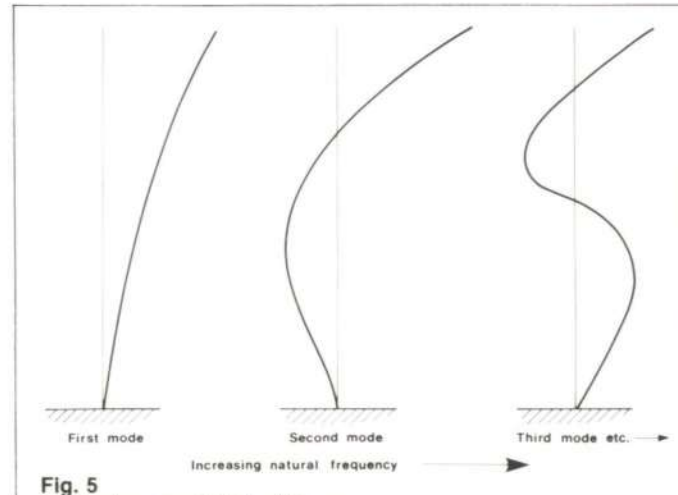

Fig. 5
Modeshapes of tall buildings

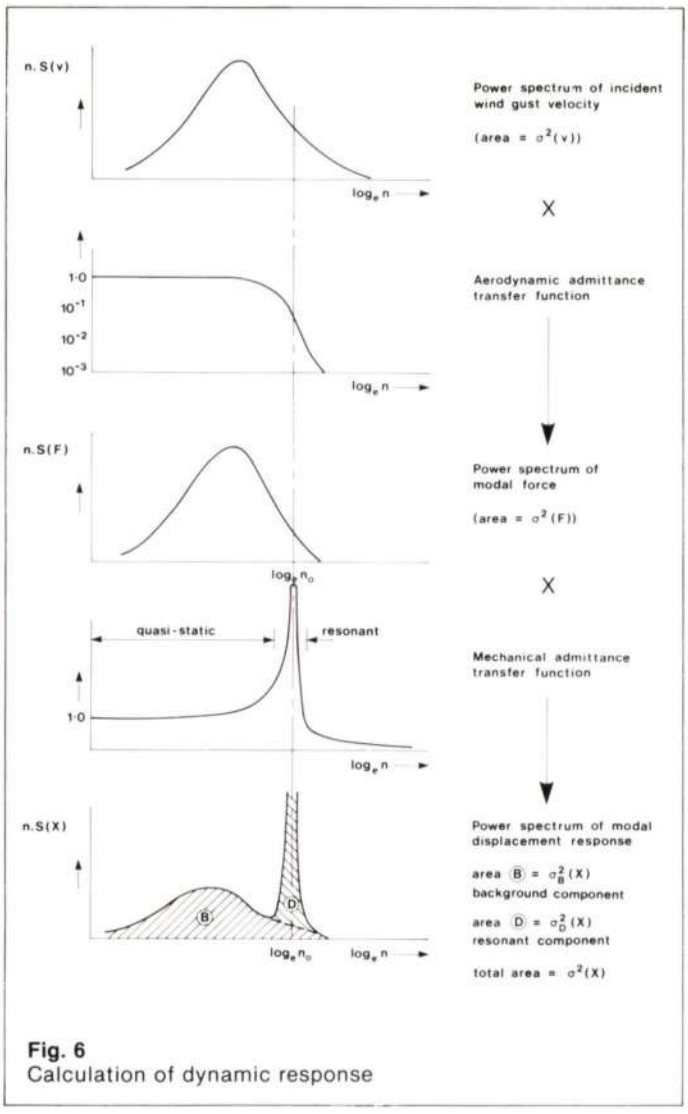

Fig. 6
Calculation of dynamic response

Generalized modal properties
It is convenient to assess the total dynamic response of buildings under wind loading in 'modal components', that is to determine the response of the structure to the fluctuating aerodynamic forces separately for each natural mode of the structure and then to combine the responses. Each mode may be a complex 3-D shape, but the analysis can be simplified by introducing the concept of generalized modal properties.

Each mode of vibration can be transformed and represented by a single generalized mass, a single generalized stiffness and a single generalized displacement, which are analogous to the parameters described above for a simple one-degree of freedom structure. The transformation ensures that the overall dynamic properties (natural frequency, vibrational energy, etc.) are unaffected but it eliminates all the degrees of freedom except one (the generalized displacement). The forcing function (aerodynamic force) is also transformed into a generalized force.

The generalized displacement, defining the magnitude of the modal response, is calculated from the generalized force and the generalized dynamic properties according to the principles given above. The deflections at specific physical points on the building are obtained by multiplying by the mode shape function μ, which defines the deflection at every point relative to the generalized displacement of the mode being considered.

The transformation procedures are briefly given in Appendix A. Warburton[2] gives a more rigorous and detailed treatment.

PREDICTION OF DYNAMIC PROPERTIES OF BUILDINGS

Estimates of the natural frequencies, modeshapes and the damping ratios of a building are pre-requisite for dynamic response predictions.

Natural frequencies and modeshapes
Natural frequencies and modeshapes are found by solving the equation

$$[\underline{K} - \underline{\omega}^2 \underline{M}]\underline{X} = O$$

where $\underline{K}$ is the stiffness matrix of the structure

$\underline{M}$ is the mass matrix

$\underline{X}$ is the modeshape vector

$\underline{\omega}^2$ is the vector of (natural circular frequencies)^2

In theory there are as many modes and frequencies in a structural system as there are degrees of freedom. In practice only the first few modes (i.e. those with the lowest frequencies) are relevant to wind response.

For practical building structures a number of approaches are possible which include:

(a) Simple methods
For normally proportioned buildings the first natural period is usually given approximately by T = H/50 seconds where H is total height in metres. This is entirely empirical but is a useful check against gross errors in more detailed assessments.

Another simple approach is given by $T = \sqrt{\delta}_{/20}$

where δ is the top deflection in mm under a distributed horizontal load equal to the weight of the building.

(b) Tabulated data
In general 'classical' solutions for elastic beams and cantilevers are of limited use for practical building forms. However, there are ESDU data items[3] which give approximate methods of predicting modes and frequencies for core or shear type building structures.

(c) Standard computer programs
The GLADYS dynamic program calculates natural modes and frequencies for core or shear type multi-storey structures, provided the modes are planar. The STAN finite element program can be used for more complex structures.

(d) Special computer programs
Some structures can be solved most effectively by making a simple lumped mass idealization. The mass matrix and stiffness matrix can be assembled and the eigen solution can be performed directly using standard matrix routines in a purpose-written program. This is illustrated in the case study.

If the more detailed methods are to prove worthwhile a number of points should be considered:

(a) How will the 'real' structural behaviour affect the stiffness (compared with simplified assumptions made for the purposes of strength design)? There may be additional framing effects, and non-structural elements may participate.

(b) For a reinforced concrete building the elastic modulus chosen should reflect dynamic loading rates.

(c) How much of the imposed load should be included in the mass of the building?

Damping
The degree of damping is difficult to predict with accuracy. Measurements on completed buildings have shown a wide variation which has in some cases been amplified by the several methods of measurement adopted.

Structural damping is caused by the hysteresis of the material of the structure, and increases with vibration amplitude as the material 'works' harder. In addition aerodynamic damping caused by the relative movement of the air and the building is present. This increases with the wind velocity. Guidance on values to be adopted for these parameters is given in ESDU 76001[4], but a more detailed ESDU data item on structural damping will soon be released.

CALCULATION OF RESPONSES

In this section the term 'response' refers to any of the following effects measured or calculated at any point of interest:

Forces or moments

Deflections

Accelerations.

A number of code methods are available, notably the along-wind response method of ESDU 76001 (available in GLADYS Dynamic) and the 'detailed method' of the National Building Code of Canada[5]. The NBCC also gives guidance on across-wind responses based empirically on aeroelastic wind tunnel studies of tall buildings. The principles of the calculations are outlined below. Similar procedures are required when using wind tunnel test measurements of aerodynamic forces to predict total responses.

Information required
It is necessary to establish:

(a) The mean hourly design wind speed. A more detailed wind climate study including directional analysis may be appropriate when using wind tunnel tests.

(b) The upstream terrain characteristics. These define the wind velocity profiles and turbulence characteristics.

(c) The dynamic properties of the building.

Mean responses
Mean forces, moments, deflections, etc., are calculated in a traditional static way, using the mean wind velocity profile and building drag coefficient. A wind tunnel test will measure the mean forces and moments directly.

Fluctuating responses
The procedure is to obtain the rms of the required response from the rms of the incident wind gusts. Since the aerodynamic and

mechanical admittances are frequency-dependent, this has to be done by considering the spectra. The complete procedure is illustrated in Fig. 6. If wind tunnel tests are used, the spectra of the aerodynamic forces will be measured, so the aerodynamic admittance is incorporated by analogue, not calculation.

The mechanical admittance is usually divided into two parts: calculating the background (or broadband or quasi-static) σ_B and the resonant (or narrow band) σ_D, components.

Several modes may contribute to the total fluctuating response. The contributions from each mode (provided the modes are sufficiently separated in period) may be combined assuming they are uncorrelated.

$$\sigma_T = \sqrt{\sigma_1^2 + \sigma_2^2 + \sigma_3^2 + \text{etc}}$$

where σ_1 etc. are the contributions from each mode.

Peak responses

Peak responses are obtained by adding extreme values of the fluctuating components to the mean response, as described in Equations 13 and 14 of David Croft's paper. The cycle frequency ν of the resonant component is the natural frequency of vibration. A lower cycle frequency is appropriate for the background components. ESDU 76001 obtains peak responses as follows:

$$\hat{E} = \bar{E} + \sqrt{[3.5\sigma_B(E)]^2 + [g\sigma_D(E)]^2}$$

where $g = \sqrt{(2\log_e n_0 T)} + \dfrac{0.577}{\sqrt{(2\log_e n_0 T)}}$

WIND TUNNEL TESTS

Reasons for wind tunnel testing

The limitations of code-based methods are obvious, since they necessarily relate to general and uniform situations. There are many instances when it is virtually impossible to estimate some of the parameters required with any degree of confidence.

Wind tunnel testing can give a more detailed and confident prediction if properly specified and conducted. The results are presented in statistical form and are suitable, in conjunction with a wind climate model, to give response level/probability predictions for limit state design based on reliability principles. Wind tunnel testing is particularly appropriate if:

(a) The building has an unusual shape, and therefore uncertain aerodynamic properties.

(b) The building has unusual dynamic characteristics such as coupled modes, strong torsion, low damping.

(c) The incident wind is difficult to characterize, e.g. major topographical features or changes in terrain roughness upstream.

(d) Surrounding tall buildings are likely to interfere by wake buffeting.

(e) Simple code methods indicate there could be a problem.

At this point it is worth bearing in mind the involvement in time and cost that a wind tunnel investigation is likely to entail, and to consider other potential sources of error that must also be tackled to make it worthwhile. The model test is only part of the procedure and the value of the end result also depends heavily on:

(a) *Wind climate data*

Mean responses increase as V^2, but purely resonant responses (e.g. acceleration) increase typically as V^3 to $V^{3.5}$. A 10% error in windspeed may therefore give a 20-30% error in peak loads and a 30-40% error in accelerations.

(b) *Structural properties*

The most difficult structural parameter to estimate is the damping. Only the resonant response is affected, but if the estimated damping is in error by a factor of 2, the acceleration level will be in error by 41%. Total loads are less sensitive because mean and background components also contribute. However, it is worthwhile examining a range of damping ratios in assessing the results.

The principal types of wind tunnel model are now discussed.

Aeroelastic models

Aeroelastic models attempt to simulate completely the interaction between the wind and the structure[6]. The building model has scaled dynamic properties (inertia, stiffness, damping) and the test is a direct analogue of full scale behaviour. In this way the total response of the building is measured, usually by a base balance, and by accelerometers in the model. There are two basic types:

(a) *Stick models*

These are rigid models mounted on gimbals at the base, as illustrated in Fig. 7. Only two (linear) translational modes can be simulated.

(b) *Multi degree-of-freedom models*

These are complex models incorporating lumped masses and stiffness elements as illustrated in Fig. 8. Torsion, coupled translation-torsion modes, and second modes can be simulated but the design and construction of such models is very involved.

The multi degree-of-freedom model is the most sophisticated method of predicting the response of a tall building. The following advantages and disadvantages should be noted.

Advantages:

(a) Direct measurement of total response
(b) Aerodynamic damping/instability effects are modelled.
(c) Complex structural properties, including effects of second modes, can be simulated.
(d) Real-time interaction between forces in different directions is obtained.

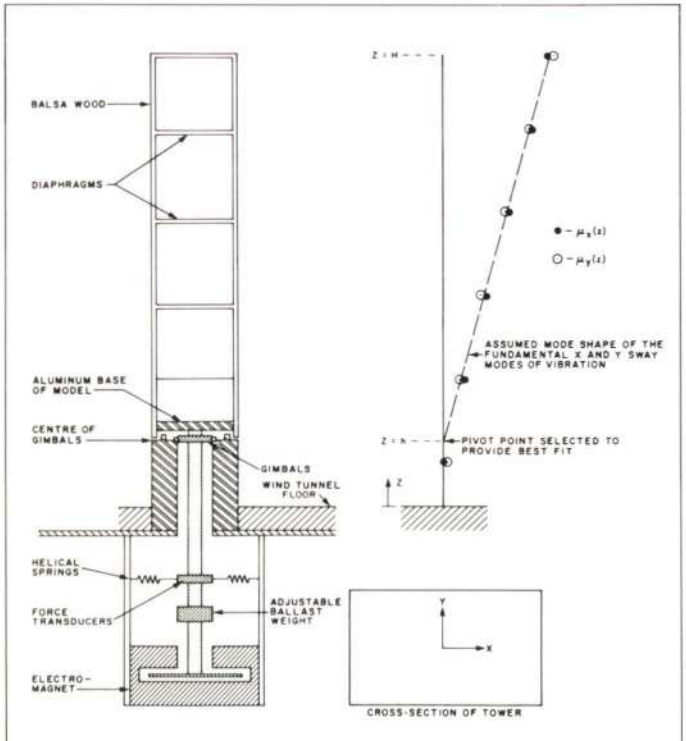

Fig. 7
Schematic representation of conventional 2 degree of freedom or 'stick' aerolastic model of tall building (after Izyumov[6])

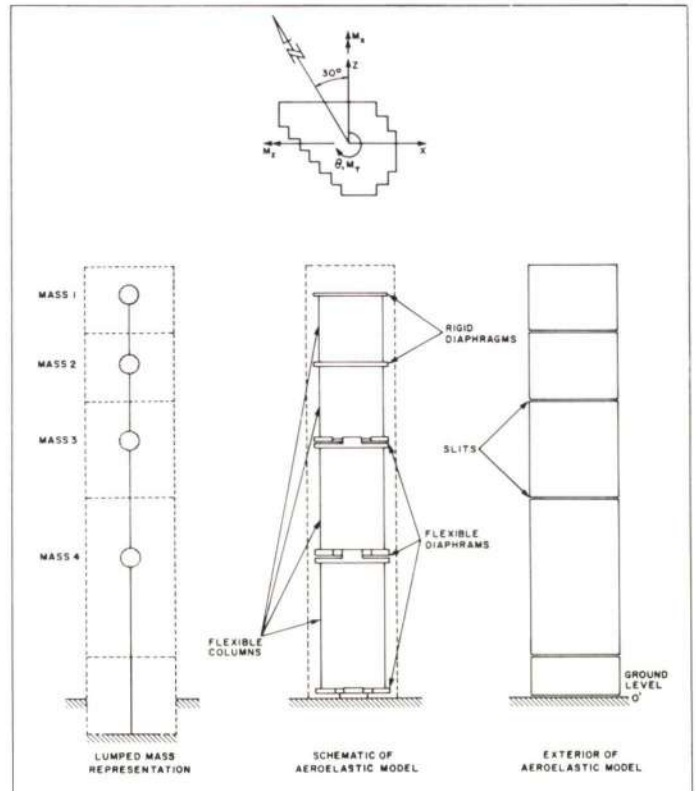

Fig. 8
Multi-degree of freedom model of tall buildings (after Izyumov[6])

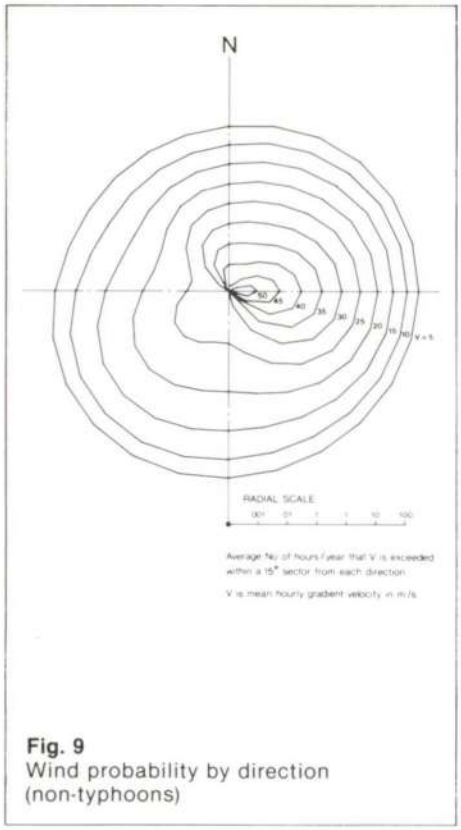

Fig. 9
Wind probability by direction (non-typhoons)

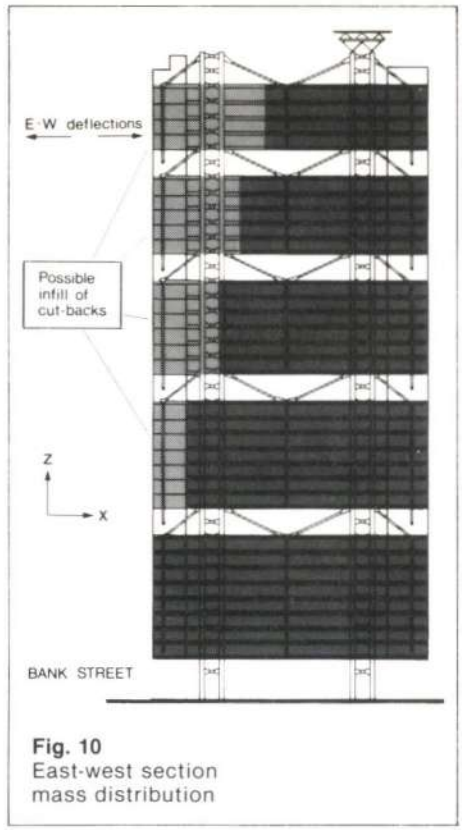

Fig. 10
East-west section mass distribution

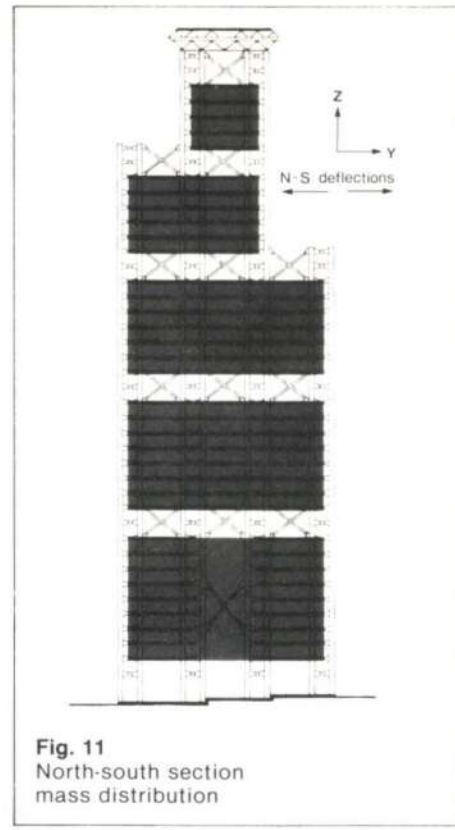

Fig. 11
North-south section mass distribution

Disadvantages:

(a) Models are time-consuming and expensive to design and construct.

(b) Considerable test time is required to obtain responses at different windspeeds and with different damping.

(c) Major changes in dynamic properties require re-testing with revised model.

Force balance method

The concept of the force balance method is to measure mean and fluctuating aerodynamic loads on a rigid model without any structural dynamic modification. The responses are then calculated, taking account of mechanical admittance using the normal mode method outlined above. The main requirement of the base balance is to measure accurately very small and rapidly fluctuating forces. This has presented design problems to achieve sufficient stiffness and sensitivity, but a number of wind tunnels now have such balances measuring from two to six directional components. The use of the five component balance of the Boundary Layer Wind Tunnel Laboratory of the University of Western Ontario is described in the case study below.

The method has many attractions

(a) Although the balance may be expensive and sophisticated, it is a standard re-useable item and the structural models for specific wind studies are simple, rigid, quickly made and inexpensive.

(b) Variations in structural properties are considered analytically, and so re-testing is not required for new damping ratios or natural modes and frequencies. Coupled modes can be dealt with.

(c) By measuring the spectra of fluctuating aerodynamic loads, testing at only one wind velocity is necessary, with consequent time saving.

Compared with a full aeroelastic study the method has the following disadvantages:

(a) Aerodynamic damping or instability are not included.

(b) Approximations are necessary in calculating the torsional response.

CASE STUDY: HONGKONG AND SHANGHAI BANK BUILDING

Introduction

The new Hongkong and Shanghai Bank headquarters building in Hong Kong has been subjected to a wind engineering study of unusually large scope and detail. The study was carried out at the Boundary Layer Wind Tunnel Laboratory of the University of Western Ontario, Canada (BLWTL), under the direction of Professor Alan Davenport. Both the terrain of Hong Kong and the form of the building itself present difficulties in using analytical methods. The scope of the study is outlined below:

(a) A wind climate study, defining a typhoon climate (for peak structural loading effects) and a non-typhoon climate (for environmental and occupant comfort related effects). See Fig. 9 and David Croft's Fig. 12.

(b) A topographical study to obtain wind profiles at the site for various incident directions. See David Croft's Fig. 9.

(c) Wind tunnel model for surface pressures.

(d) Wind tunnel model for overall aerodynamic forces (force balance technique).

(e) Environmental wind tests.

This work is documented in a series of BLWTL reports[7], from which much of the following data is taken.

The subsequent sections describe the use of base balance measurements to obtain design results.

Dynamic properties of the building

The general arrangement of mass in the building is illustrated in Figs. 10 and 11. The structure is designed to accommodate future infilling of the 'set backs' on the east side (Fig. 10) and consequently the primary structure is essentially symmetrical about the central N-S axis. Since the centre of mass becomes offset from this axis in the higher zones of the currently proposed building, significant lateral torsional behaviour is present in all the modeshapes (Fig. 12). All the first modes have approximately linear elevational shapes.

The modes and frequencies were obtained by analyzing a notional five lumped mass model as illustrated in Fig. 13. Each mass has three degrees of freedom, (in the x, y and torsion directions). A flexibility matrix was obtained for the 15 degree of freedom system by analyzing a detailed finite element model of half the structure under a series of unit loads applied at the mass centre levels. This was transformed and inverted to give a stiffness matrix (K) relating forces to deflections for the total of 15 degrees of freedom at the centre of mass locations. Modeshapes and frequencies were obtained by direct eigensolution of the equation

$$[\underline{K} - \omega^2 \underline{M}]\underline{X} = 0 \qquad \text{where } \underline{M} \text{ is the diagonal mass matrix}$$

using a purpose written program incorporating standard matrix routines. This enabled the effect of mass asymmetry to be quantified without developing a much larger finite element model of the whole building. Changes in mass distribution (e.g. infilling the east side) could also be examined easily.

Damping was estimated to lie between 1% and 2% of critical, based on previous experience of steel-framed buildings. The lower value was adopted for design predictions.

Test details

From the wind tunnel studies with a 1:2500 scale topographical model of Hongkong and its surrounds, five upstream wind categories were identified to cover all wind directions at the site (David Croft's Fig. 9). The pronounced sheltering of the site for winds from the south and south-west is evident.

A rigid, light architectural model of the building at 1:500 scale was mounted on BLWTL's 5-component base balance at the centre of a proximity model, which included detailed representation of all features within a 600m radius of the site. The whole assembly was mounted on a turntable in the wind tunnel. Wind profiles and turbulence characteristics measured in the 1:2500 topographical study were simulated at this larger scale to produce appropriate wind conditions at the site for each prevailing wind direction.

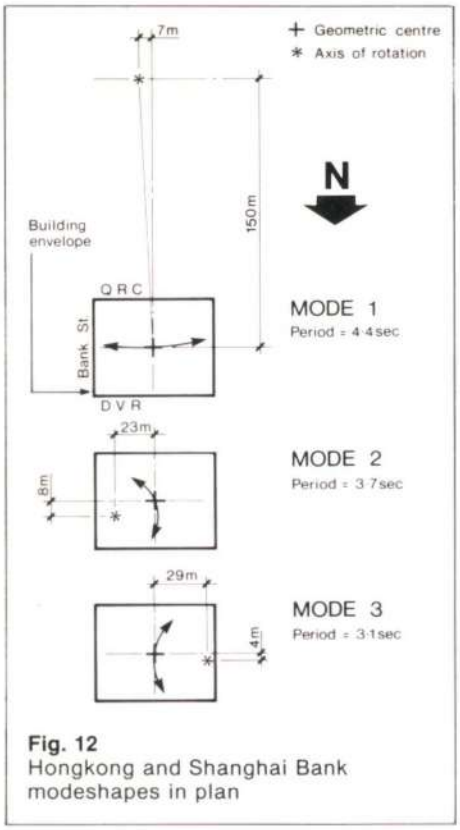

Fig. 12
Hongkong and Shanghai Bank modeshapes in plan

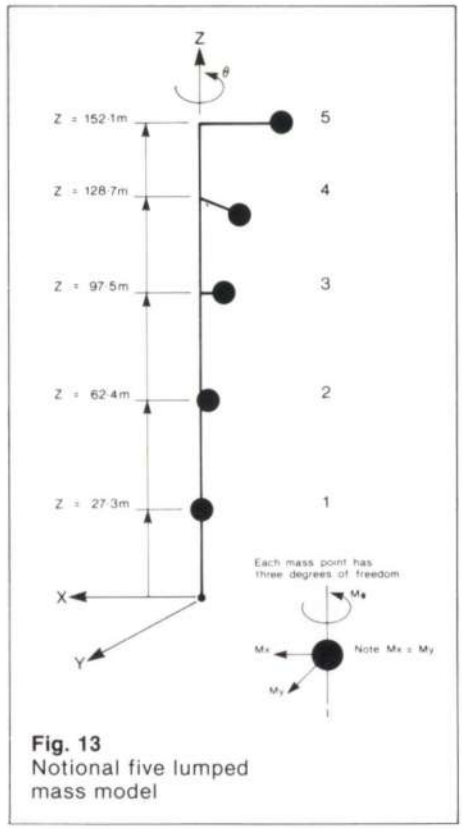

Fig. 13
Notional five lumped mass model

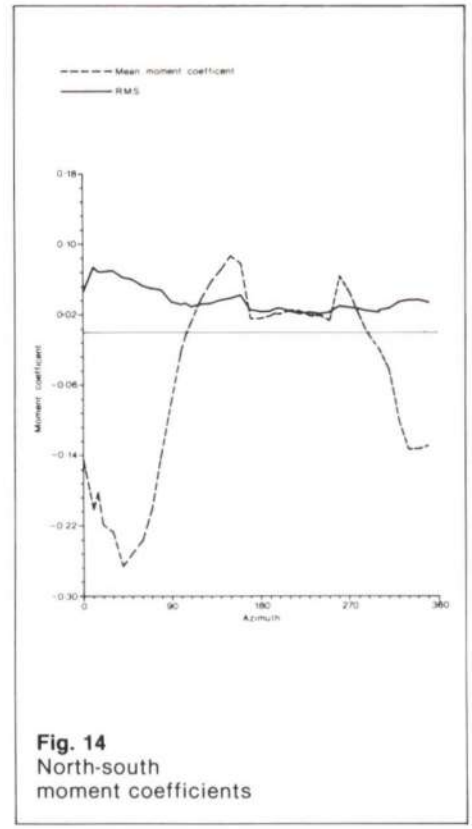

Fig. 14
North-south moment coefficients

Base balance measurements

Base forces in the model were measured for winds from each direction at 15° azimuth intervals and presented as mean and rms fluctuating components normalized as coefficients to enable full-scale forces to be determined. Spectra of the fluctuating components were measured for key directions.

The five components measured were:

(a) N-S overturning moment
(b) E-W overturning moment
(c) N-S shear force
(d) E-W shear force
(e) Torsion moment.

Details of the balance are given in Tchanz[8].

A typical plot of mean and rms coefficients against azimuth is given in Fig. 14. These are aerodynamic forces only, with no structural dynamic magnifications. Full scale forces and moments are obtained as:

$$F_X = C_{FX} . W_X . H . q_g$$
$$M_X = C_{MX} . W_X . H^2 . q_g$$
$$T = C_T . W_X . W_Y . H . q_g$$

where F_X, M_X, T are shear force, moment and torque
C_{FX}, C_{MX}, C_T are the corresponding coefficients
W_X, W_Y, H are the widths and height of the building
$q_g = \frac{1}{2} \rho V_g^2$ = dynamic wind pressure at gradient height.

A typical spectrum (as measured) is shown in Fig. 15. This is smoothed for 'noise' and corrected for mechanical resonances of the test equipment and electrical filtering characteristics before use in predictions.

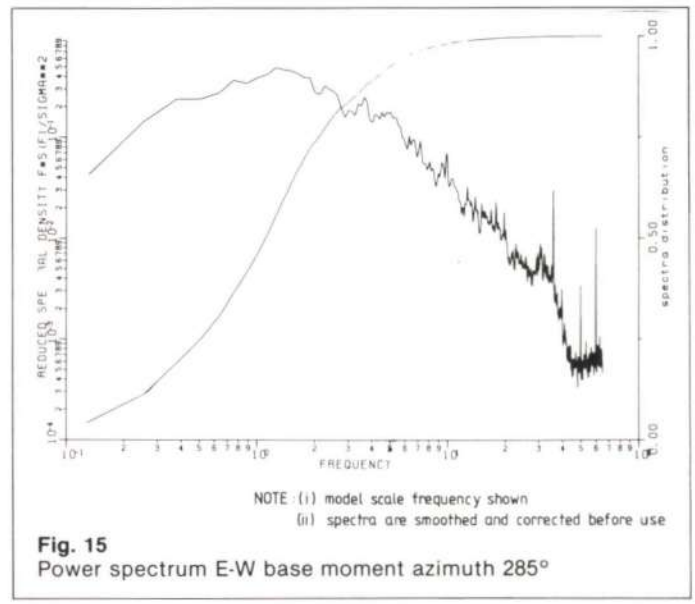

Fig. 15
Power spectrum E-W base moment azimuth 285°

Prediction of structural responses

A detailed description of the analysis of responses is given in Appendix A. The key concept to note is that for a modeshape linear in elevation the mode generalized *force* is directly proportional to the base bending *moment* measured in the wind tunnel.

Fig. 16 shows the variation of peak acceleration with azimuth and windspeed. Fig. 17 shows the variation of base moment with azimuth, windspeed and damping. Similar results can be obtained for other responses.

Frequency of occurrence of response levels

Having established response/azimuth/windspeed relationships the wind climate model is introduced to make predictions of the frequency of exceedance of chosen response levels.

To illustrate the procedure, Fig. 9 shows the number of hours per year that Vg values are exceeded (by azimuth) in the non-typhoon model. From Fig. 16 it is possible to establish for each azimuth the values of Vg required to cause a specific response level to be exceeded. It is therefore possible to predict the total number of hours per year that the response will be exceeded.

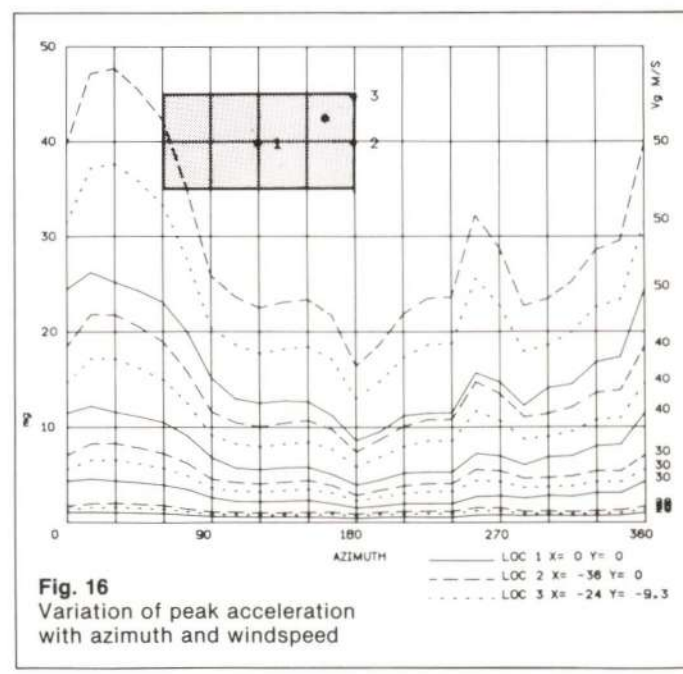

Fig. 16
Variation of peak acceleration with azimuth and windspeed

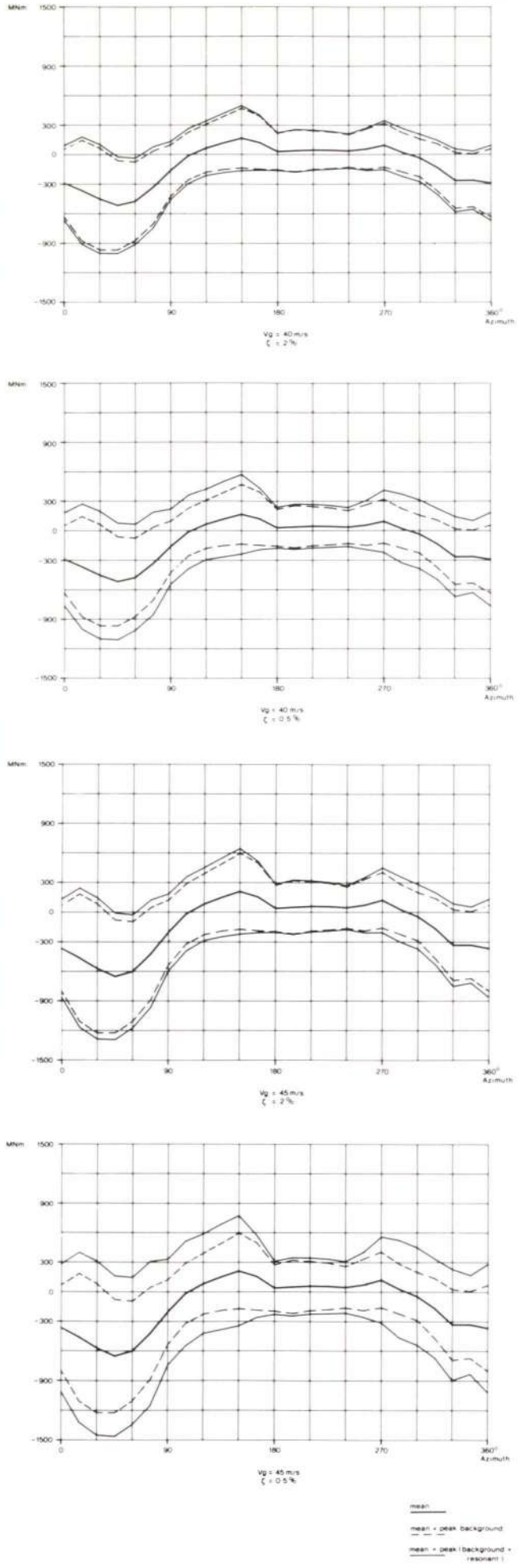

Fig. 17
Hongkong and Shanghai Bank
variation of N-S moment response
with windspeed and damping

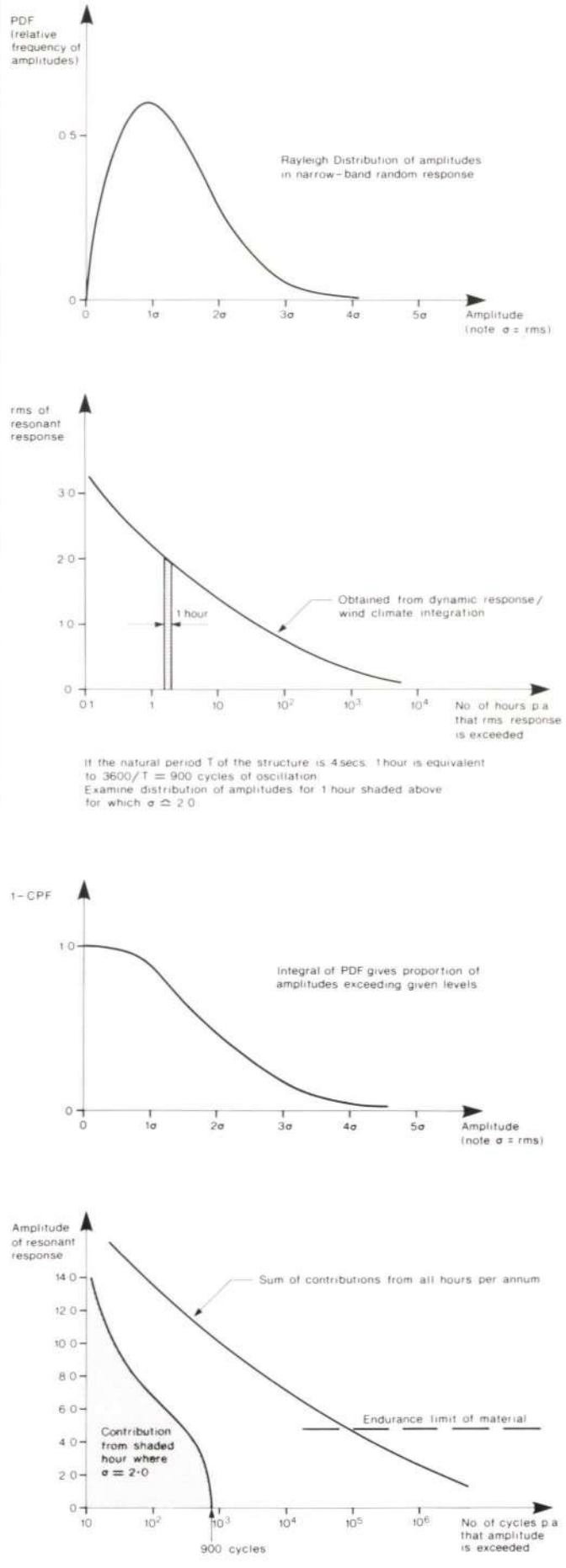

Fig. 18
Development of fatigue load

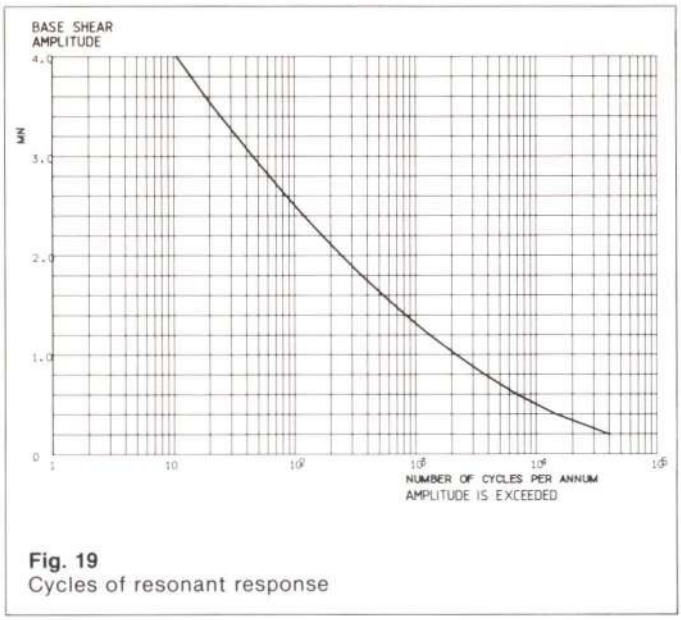

Fig. 19
Cycles of resonant response

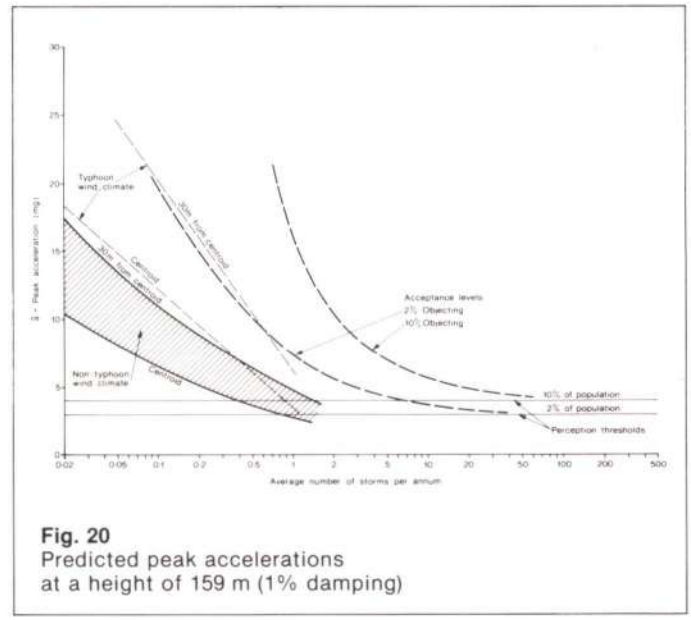

Fig. 20
Predicted peak accelerations
at a height of 159 m (1% damping)

This data can then be used to predict:

(a) Return periods of peak loading effects. This involves the cycle frequency of the wind to obtain the number of hours that constitute an independent storm or 'event', as described in David Croft's paper.

(b) The number of cycles of oscillation at particular amplitude levels each year, for use in fatigue assessments. In this case only the resonant response component makes a significant contribution. There are 3600/T cycles of oscillation per hour (where T = natural period in seconds) and for each rms response level there is a known (Rayleigh) distribution of individual amplitude peaks. This enables the total number of cycles in each amplitude range to be determined, as in Fig. 18.

Fig. 19 shows the number of cycles per annum of base shear amplitudes, and Fig. 20 the variation of peak acceleration with return period.

Member design

A number of approaches are possible to obtain design loads for individual members. (In the case of the Hongkong and Shanghai Bank project the peak base force responses were significantly lower than those obtained by applying the Hong Kong statutory wind pressures, and the statutory loads were used for the strength design.) Although the force balance method does not define fully the distribution of effective loading with height, the ratio of peak moment to peak shear gives an effective centre of loading. This can be augmented by integrating mean pressures obtained from a pressure tapped model to give an estimate of the mean load distribution. The resonant component distribution can be obtained by consideration of the inertia forces. An 'effective' quasi-static loading diagram can be put together from these components, and a normal static analysis used to obtain individual member forces. The combination of simultaneous loading from two translational and the torsional directions has been studied using aeroelastic models by BLWTL who recommend the following combinations as design loadcases:

(1) $1.0F_x$ or $1.0F_y$

(2) $0.8F_x \pm 0.8F_y$

(3) $0.6F_x \pm 0.6F_y \pm 0.6F_\theta$

where Fx, Fy, F_θ are the member load effects obtained under peak x, y and θ effective loads acting alone.

An alternative approach, possible for simple structural forms, is to use the modal analysis directly. There is a relationship (influence coefficient) between any member force and the generalized displacement of a particular mode, just as there is for an overall base shear or corner acceleration. Therefore a member force can be treated in exactly the same way as a base shear and the variation of peak member force with return period can be obtained directly by considering all the relevant modes.

Occupant comfort

The acceleration responses at the top of the building are given in Fig. 20, together with the acceptance criteria proposed by Davenport. It can be seen that for frequent events the acceptable level is the threshold of perception for a small proportion of the occupants, whereas for rare events limited perceptible motions are considered acceptable. It has to be borne in mind that acceleration predictions are very sensitive to a number of input parameters, and should be considered as indicative only. Comfort criteria also are indicative, based on subjective reactions of building occupants to infrequent events. Davenport's criteria are in line with other workers' recommendations.

In Hong Kong typhoons are associated with strong winds and damage and for this reason occupant reactions to building movement will be different from those in normal operating conditions; typhoons have therefore been disregarded for comparison with normal acceptance criteria. It can be seen that the expected performance of the building under non-typoon winds is good.

References

(1) LAWSON, T.V. Wind effects on buildings: Volume 1: Design applications. Applied Science Publishers, 1980.

(2) WARBURTON, G.B., The dynamical behaviour of structures, Pergamon Press, 1964.

(3) ESDU data items
79005, Undamped natural vibration of shear buildings.
81036, Undamped natural vibration of core buildings.
82019, Undamped natural vibration of sway frame buildings and frame structures.

(4) ESDU data item 76001, The response of flexible structures to atmosphere turbulence

(5) NATIONAL Building Code of Canada, Ottawa, 1980 and Supplement to NBC 1980.

(6) IZYUMOV, N. The aeroelastic modelling of tall buildings, Proc. International Workshop on Wind Tunnel Testing. U.S. National Bureau of Standards, 1982.

(7) DAVENPORT, A.G., *et al.* BLWTL Reports on the Hongkong and Shanghai Bank Project. (Copies held by Michael Willford)

(8) TCHANZ, T. Measurement of total dynamic loads using elastic models with high natural frequencies. Proc. International Workshop on Wind Tunnel Testing. U.S. National Bureau of Standards, 1982.

APPENDIX A: CALCULATION OF TOTAL RESPONSES BY THE NORMAL MODE METHOD

Introduction

This appendix describes the transformations required to obtain generalized modal properties and illustrates how the normal mode method can be used to predict total responses using the results of base force balance measurements on a rigid model in a wind tunnel test.

Notation

In some cases simplified notation is used in order to reduce complexity in the various equations.

	Full notation	Simplified notation
Height of building	H	
Height	z	
Frequency of mode j	n_j	n
Mode shape of mode j on a reference axis		
x Component	$\mu_{xj}(z)$	μ_x
y Component	$\mu_{yj}(z)$	μ_y
θ Component	$\mu_{\theta j}(z)$	μ_θ

Mode shape at a particular node not on reference axis		
x Component	ψ_{xj}	ψ_x
y Component	ψ_{yj}	ψ_y
θ Component	$\psi_{\theta j}$	ψ_θ
Values of μ at z = H		
x Component	a_{xj}	a_x
y Component	a_{yj}	a_y
θ Component	$a_{\theta j}$	a_θ
Mass/unit height	$m(z)$	m
Rotational inertia/unit height	$m_\theta(z)$	m_θ
Wind load/unit height		
x Component	$w_x(z,t)$	w_x
y Component	$w_y(z,t)$	w_y
θ Component	$\tau(z,t)$	τ
Generalized Mass in mode j	M_j	
Generalized Stiffness in mode j	K_j	
Background gust factor	g_B	
Resonant gust factor	g_R	
Critical damping ratio	ζ	
Cycle frequency	ν	

The following quantities which vary with time are treated in terms of mean, RMS and power spectral density values.

	Inst. Value at time t	Mean	RMS	PSD at freq. n
Generalized Force	$F_j(t)$	$\bar{F}_j$	σ_{Fj}	$S_{Fj}(n)$
Base balance forces:				
Force in x-dirn	$F_{xB}(t)$	$\bar{F}_{xB}$	σ_{FxB}	$S_{FxB}(n)$
Force in y-dirn	$F_{yB}(t)$	$\bar{F}_{yB}$	σ_{FyB}	$S_{FyB}(n)$
Moment about x-axis	$M_{xB}(t)$	$\bar{M}_{xB}$	σ_{MxB}	$S_{MxB}(n)$
Moment about y-axis	$M_{yB}(t)$	$\bar{M}_{yB}$	σ_{MyB}	$S_{MyB}(n)$
Torque	$M_{\theta B}(t)$	$\bar{M}_{\theta B}$	$\sigma_{M\theta B}$	$S_{M\theta B}(n)$
Generalized displacement in mode j	$A_j(t)$	$\bar{A}_j$	σ_{ABJ} (background), σ_{ARJ} (resonant)	
X-displacement in mode j	$X_j(t)$	$\bar{X}$	σ_x	
Y-displacement in mode j	$Y_j(t)$	$\bar{Y}$	σ_y	
Rotation in mode j	$\theta_j(t)$	$\bar{\theta}$	σ_θ	
x-acceleration	$\ddot{x}(t)$		$\sigma_{\ddot{x}}$	
y-acceleration	$\ddot{y}(t)$		$\sigma_{\ddot{y}}$	
θ-acceleration	$\ddot{\theta}(t)$		$\sigma_{\ddot{\theta}}$	

Modal analysis

The first step is to carry out a dynamic modal analysis of the structure to determine the frequencies and mode shapes of the structure in free vibration.

Generalized quantities

The response of a structure to wind excitation is most easily solved by considering generalized quantities as described below. The method is merely stated here and, for further information, reference should be made to the literature.

The instantaneous *Generalized Force* $F_j(t)$ corresponding to mode j is defined in terms of the applied loads w and τ and the mode shape μ:

$$F_j(t) = \int_0^H w_x \mu_x dz + \int_0^H w_y \mu_y dz + \int_0^H \tau \mu_\theta dz \quad (1)$$

In this expression the mode shape and the forces should relate to the reference axis system, for example the geometric centre axis of the building. (The mode shapes need not be normalized).

If a force balance test is carried out then the generalized force can be obtained from the test results, as described in the section below on determination of generalized force.

The *Generalized Mass* M_j corresponding to mode j is calculated from the mass and rotational inertia per unit height and the mode shape μ thus:

$$M_j = \int_0^H m\mu_x^2 dz + \int_0^H m\mu_y^2 dz + \int_0^H m_\theta \mu_\theta^2 dz \quad (2)$$

In this expression it is assumed that the centre of mass is on the reference axis at all levels. If this is not the case the following more general expression (expressed here for simplicity for a lumped mass model) should be used:

$$M_j = [\mu_j]^T [M] [\mu_j] \quad (3)$$

where $[\mu_j]$ is the vector of node displacements defining the mode shape and [M] is the mass matrix (containing off-diagonal terms as appropriate) with respect to the reference axis.

The *Generalized Stiffness* K_j corresponding to mode j is related to the generalized mass thus

$$K_j = (2\pi n_j)^2 M_j \quad (4)$$

where n_j is the frequency of that mode.

The instantaneous *Generalized Displacement* $A_j(t)$ corresponding to mode j is found from the generalized force and stiffness thus

$$A_j(t) = F_j(t)/K_j \quad (5)$$

The generalized displacement varies with time and can be considered in three components:

(a) A mean value $\bar{A}_j$ which is given by

$$\bar{A}_j = \frac{\bar{F}_j}{K_j} \quad (6)$$

(b) A fluctuating component due to the background (or broadband) excitation. This is caused by the turbulence of the wind loading, in other words the gusts, and occurs irrespective of any dynamic response of the structure. The background RMS value of $A_j(t)$ is given by

$$\sigma_{ABj} = \sigma_{Fj}/K_j \quad (7)$$

(c) A fluctuating component due to the resonance of the structure. The RMS of this is given by

$$\sigma_{ARj} = \sqrt{\frac{\pi}{4\zeta K^2_j} n_j S_{Fj}(n_j)} \quad (8)$$

where ζ is the critical damping ratio and S_{Fj} is the power spectral density (PSD) of F(t) at the frequency n_j of the mode under consideration.

In order to calculate the mean and RMS values of the generalized displacement it is necessary to determine the mean, RMS and PSD of the generalized force F. This is discussed in the next section.

Determination of generalized force

Generalized aerodynamic forces can be estimated analytically or by performing wind tunnel tests. This section describes how generalized forces in mean, RMS and PSD components are determined from the results of force balance measurements on a rigid model in a wind tunnel test, (in which no structural dynamic effects are modelled). The base forces and moments measured are purely aerodynamic forces which can be expressed as:

Force in x-dirn $$F_{xB}(t) = \int_0^H w_x dz \quad (9)$$

Force in y-dirn $$F_{yB}(t) = \int_0^H w_y dz \quad (10)$$

Moment about x-axis $$M_{xB}(t) = \int_0^H w_y z dz \quad (11)$$

Moment about y-axis $$M_{yB}(t) = \int_0^H w_x z\,dz \qquad (12)$$

Torque $$M_{\theta B}(t) = \int_0^H \tau\,dz \qquad (13)$$

Mean, RMS and PSD values are measured. In practice they are measured in model scale units but can then be factored up to full scale values, and it is the latter that are referred to here.

Usually most of the contribution of the response of a tall building comes from the three fundamental, 'first' modes. Each fundamental mode may contain x, y and θ components in its mode shape (if coupling is present) and for each such mode the generalized force can be estimated by assuming a linear form for the x and y components and a constant value for the θ component, i.e.,

$$\mu_x = \frac{z a_x}{H} \qquad \mu_y = \frac{z a_y}{H} \qquad \mu_\theta = a_\theta \qquad (14)$$

where a_x, a_y, a_θ are the values of μ_x, μ_y, μ_θ respectively at $z = H$.

Substituting in Equation (1)

$$F_j(t) = \frac{a_x}{H}\int_0^H w_x z\,dz + \frac{a_y}{H}\int_0^H w_y z\,dz + a_\theta \int_0^H \tau\,dz$$

$$= \frac{a_x}{H} M_{yB}(t) + \frac{a_y}{H} M_{xB}(t) + a_\theta M_{\theta B}(t) \qquad (15)$$

The mean, RMS and PSD values of F can thus be expressed in terms of the mean, RMS and PSD values of the base balance readings. The mean value is given by:

$$\bar{F}_j = \frac{a_x}{H}\bar{M}_{yB} + \frac{a_y}{H}\bar{M}_{xB} + a_\theta \bar{M}_{\theta B} \qquad (16)$$

It is usually found that there is little correlation between the three components, so that the RMS of F is given by:

$$\sigma^2_{F_j} = \left(\frac{a_x}{H}\right)^2 \sigma^2_{MyB} + \left(\frac{a_y}{H}\right)^2 \sigma^2_{MxB} + a^2_\theta \sigma^2_{M\theta B} \qquad (17)$$

For the power spectral density, noting that

$$\int_0^\infty S_{F_j}(n)\,dn = \sigma^2_{F_j} \qquad \int_0^\infty S_{MxB}(n)dn = \sigma^2_{MxB} \quad \text{etc}$$

and substituting in Equation (17) then

$$\int_0^\infty S_{F_j}(n)\,dn = \left(\frac{a_x}{H}\right)^2 \int_0^\infty S_{MyB}(n)dn + \left(\frac{a_y}{H}\right)^2 \int_0^\infty S_{MxB}(n)dn + a^2_\theta \int_0^\infty S_{n\theta B}(n)\,dn$$

from which it follows

$$S_{F_j}(n) = \left(\frac{a_x}{H}\right)^2 S_{MyB}(n) + \left(\frac{a_y}{H}\right)^2 S_{MxB}(n) + a^2_\theta S_{M\theta B}(n) \qquad (18)$$

Node displacements

Having calculated the generalized displacements for each mode, the displacements of individual nodes can be found.

The instantaneous displacement of a given node corresponding to mode j is given by:

$$\left.\begin{aligned} x_j(t) &= A_j(t)\psi_{xj} \\ y_j(t) &= A_j(t)\psi_{yj} \\ \theta_j(t) &= A_j(t)\psi_{\theta j} \end{aligned}\right\} \qquad (19)$$

Here the mode shape ψ relates to the node under consideration as opposed to that of the force origin μ. ψ is related to μ at the same level by an orthogonal transformation.

Combining the contributions from all modes the mean values are then given by

$$\left.\begin{aligned} \bar{x} &= \Sigma(\bar{A}_j\psi_{xj}) \\ \bar{y} &= \Sigma(\bar{A}_j\psi_{yj}) \\ \bar{\theta} &= \Sigma(\bar{A}_j\psi_{\theta j}) \end{aligned}\right\} \qquad (20)$$

where the summation is for all modes considered. The RMS deflections are given by

$$\left.\begin{aligned} \sigma_x &= \sqrt{|\Sigma(\sigma_{ABj}\psi_{xj})^2 + \Sigma(\sigma_{ARj}\psi_{xj})^2|} \\ \sigma_y &= \sqrt{|\Sigma(\sigma_{ABj}\psi_{yj})^2 + \Sigma(\sigma_{ARj}\psi_{yj})^2|} \end{aligned}\right\} \qquad (21)$$

etc

Equations (21) imply zero correlation between the background and resonant response and also between the different modes. This is normally found to be a reasonable assumption.

The expected maximum (or peak) values are given by

$$\left.\begin{aligned} x_{max} &= \bar{x} + \sqrt{|\Sigma(g_B\sigma_{ABj}\psi_{xj})^2 + \Sigma(g_R\sigma_{ARj}\psi_{xj})^2|} \\ y_{max} &= \bar{y} + \sqrt{|\Sigma(g_B\sigma_{ABj}\psi_{yj})^2 + \Sigma(g_R\sigma_{ARj}\psi_{yj})^2|} \end{aligned}\right\} \qquad (22)$$

etc.

The peak factors g_B and g_R for the background and resonant components are given by

$$g = \sqrt{(2\log_e \nu T)} + \frac{0.577}{\sqrt{(2\log_e \nu T)}} \qquad (23)$$

where ν is the cycle frequency and T is the length of time considered (usually one hour, i.e. 3600 secs).

For the resonant component, ν is taken as the frequency n_j of the mode considered which leads to values of g_R in the range 3.5-4.5.

For the background component, ν is given theoretically by

$$\nu^2 = \frac{\int_0^\infty n^2 S_{Fj}(n)\,dn}{\int_0^\infty S_{Fj}(n)\,dn} \qquad (24)$$

but is usually taken as a constant 3.5 which is a typical average value given by Equation (24).

Node accelerations

The mean values of all the accelerations will, of course, be zero. The RMS acceleration of a node can be obtained from the resonant generalized displacement RMS thus

$$\sigma_{\ddot{x}} = \sqrt{|\Sigma(\sigma_{ARj}\psi_{xj}4\pi^2 n_j^2)^2|} \qquad (25)$$

etc.

The expected maximum values are then

$$\ddot{x}_{max} = \sqrt{|\Sigma(g_R\sigma_{ARj}\psi_{xj}4\pi^2 n_j^2)^2|} \qquad (26)$$

where g_R is as defined in section above on node displacements.

Node inertia forces

The RMS inertia forces caused by the acceleration of the structure can be found from the node accelerations thus

$$\begin{bmatrix}\sigma_{PR\ddot{X}}\\ \sigma_{PR\ddot{Y}}\\ \sigma_{PR\ddot{\theta}}\end{bmatrix} = [M]\begin{bmatrix}\sigma_{\ddot{x}}\\ \sigma_{\ddot{y}}\\ \sigma_{\ddot{\theta}}\end{bmatrix} \qquad (27)$$

where the accelerations are evaluated using Equations (25) and the mode shapes μ of the reference axis, and [M] is the mass matrix as used in Equation (3).

Base shears and moments

The base forces and moments in each mode will also be made up of mean, background and resonant components. The mean and background components are given directly by the balance measurements. The resonant components can be simply obtained by summing the inertia forces given by Equation (27) up the building for each node in turn. The RMS resonant base shears and moments for mode j are then given (for a lumped mass model) by

$$\begin{bmatrix}\sigma_{FxRj}\\ \sigma_{FyRj}\\ \sigma_{MxRj}\\ \sigma_{MyRj}\\ \sigma_{M\theta Rj}\end{bmatrix} = (2\pi n_j)^2 \sigma_{ARj} \Sigma \begin{bmatrix}1&0&0\\0&1&0\\0&z&0\\z&0&0\\0&0&1\end{bmatrix} [M] \begin{bmatrix}\mu_x\\ \mu_y\\ \mu_\theta\end{bmatrix} \qquad (28)$$

where [M] and z are the mass matrix and height of a lumped mass and the summation is for all the lumped masses.

The RMS values are then given by equations of the form

$$\sigma^2_{Fx} = \sigma^2_{FxB} + \Sigma(\sigma^2_{FxRj}) \qquad (29)$$

where the summation is for all modes.

The expected maximum values are similarly given by

$$F_{x\,max} = \bar{F}_{xB} + \sqrt{|(g_B\sigma_{FxB})^2 + \Sigma(g_R\sigma_{FxRj})^2|} \qquad (30)$$

where g_B and g_R are as defined in the section on node displacements.

Arup Ideas Competition

First prize:
'The Red Balloon'
Alastair Hughes

In April this year an Ideas Competition, thought up by Stuart Richardson of Building Engineering Group 2, was held with over £1,000 prize money on offer for designs for the most original pavilion at Expo' 89 in Paris. (This was before the Expo was cancelled.) There were 83 entries, from which 11 were chosen at the preliminary judging stage in June to go forward to the second stage, when the successful ones were required to develop their ideas on a maximum of three sheets of A1 paper. The competition closed on 1 August, when the entries were given to two architects, Terry Farrell and Tom Heneghan who acted as guest judges. Their decision came within a few days and in late September the winning designs were put on display.
The top six are featured here, together with the judges' comments.

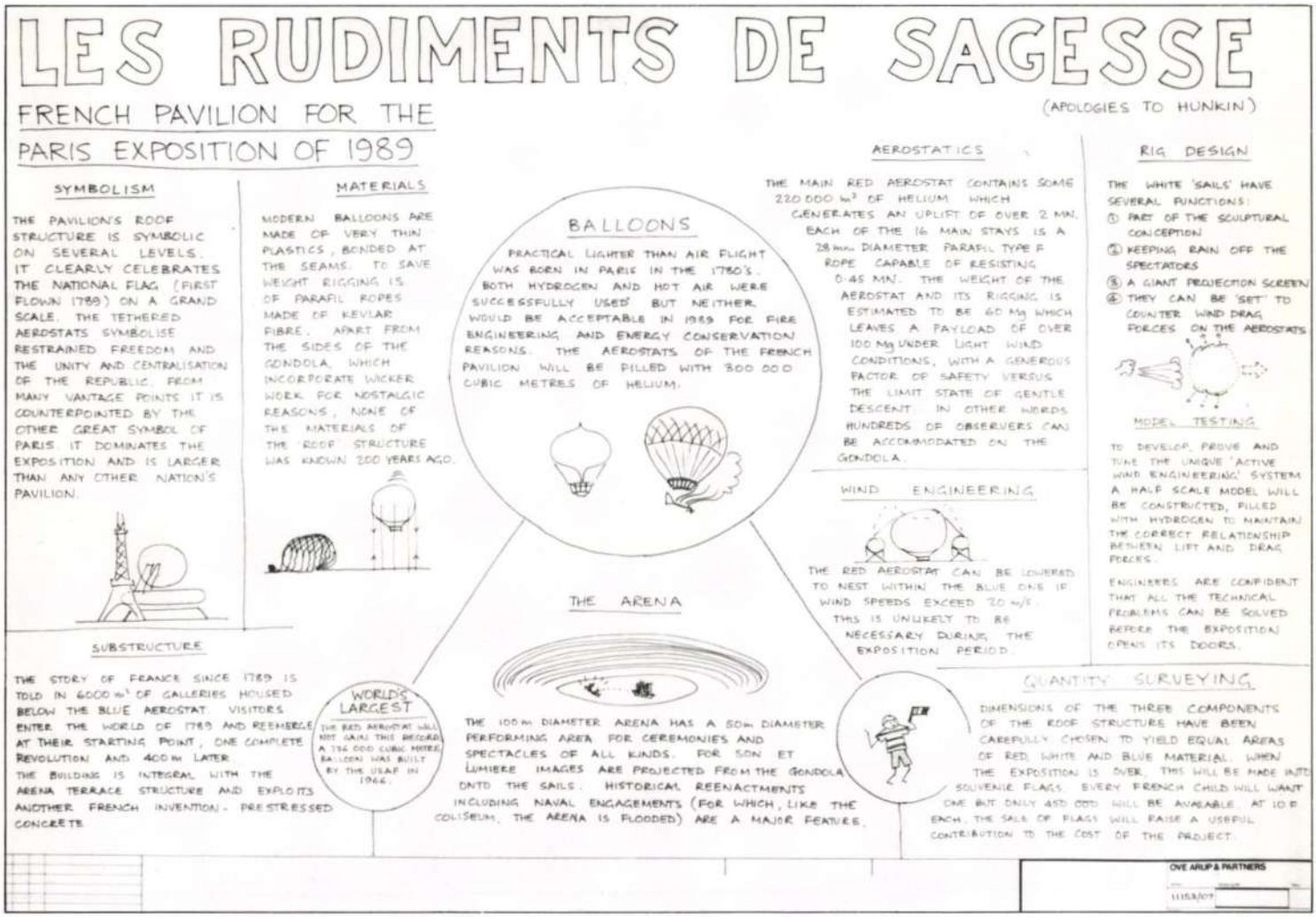

A simple idea, the simplicity of which would translate into reality. Very well presented, both at the basic communication level and graphically (without resorting to extraordinary draughtsmanship); the key notions are very effectively explained. The building would be so simple and memorable (and beautiful). Brilliantly resolves the question of future use under the paragraph 'Quantity Surveying' – a heading so resoundingly dull and inappropriate that it drew the eye immediately. Engineering prowess is also demonstrated in this entry, but not at the expense of popular imagery. The idea of making flags from the balloons appeals enormously – as the huge red symbol would after the event be distributed through the country. A very symbolic gesture, as indeed the whole concept is strong symbolically and very appropriate for an international Expo.

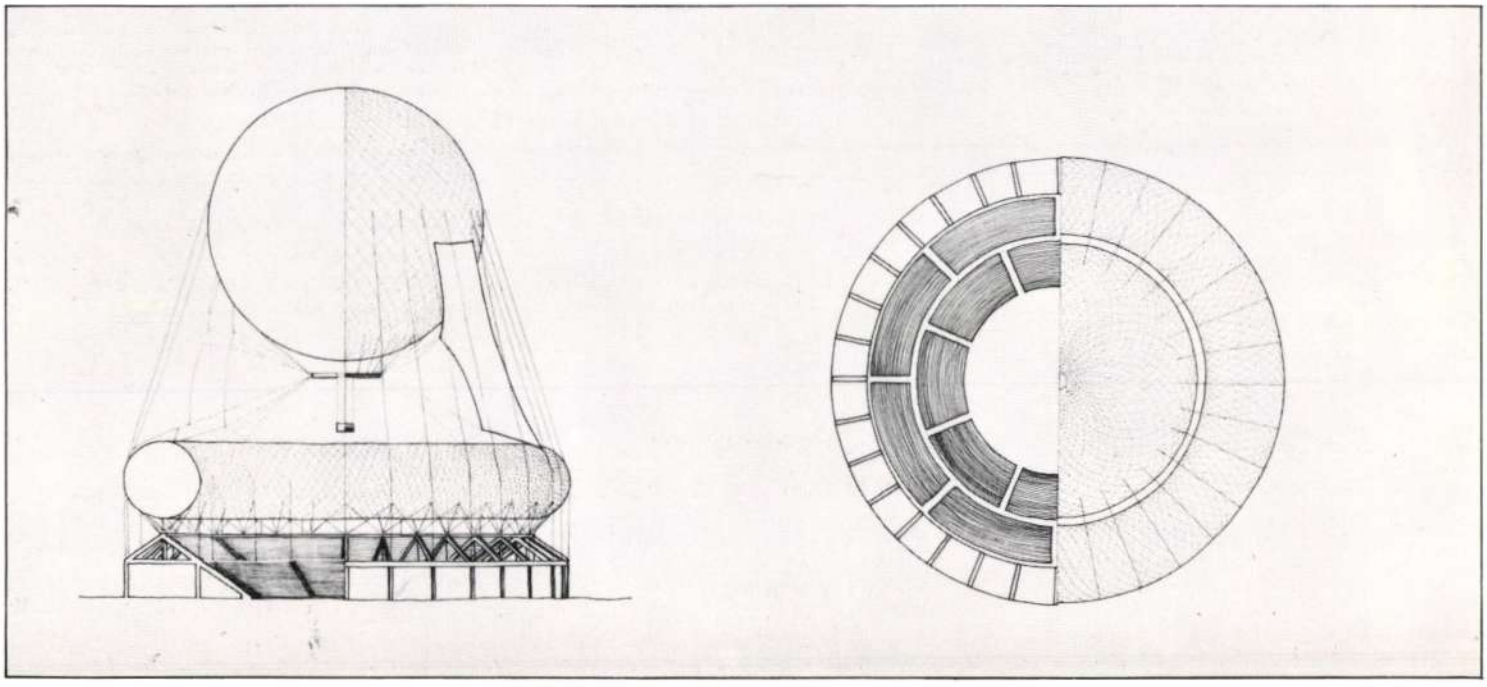

The idea is for a helium filled roof structure to cover the host nation's pavilion and act as a landmark and 'symbol' for the exposition as a whole.

Conceived on a large scale (as host nation, France do'es not feel bound by the 4000 m² restriction) it covers a terraced arena which seats over 10000 spectators for ceremonial events, concerts and performances.

The perimeter of the arena, conventional in structure, houses a sequence of national exhibits round the circle.

The roof itself has two separate helium filled volume's. The upper one is simply a red balloon of the 'normal' spherical kind. The lower one, toroidal in form, acts as a compression ring by virtue of slight positive pressurization. It's fabric is 'blue'. It floats directly above the perimeter building.

The space between the red and blue volumes is filled by adjustable fabric 'sails', white in colour. These can be furled on fine days and unfurled when protection from rain is required. The 'mechanisms' used are adaptations of commonly used yacht equipment.

The sails are not designed to provide total weather exclusion. Their purpose is to shed the rain and, of course, to act as part of the 'display' aspect of the building. In strong wind conditions certain of the sails can be set to reduce the downwind drag and hence the stay forces.

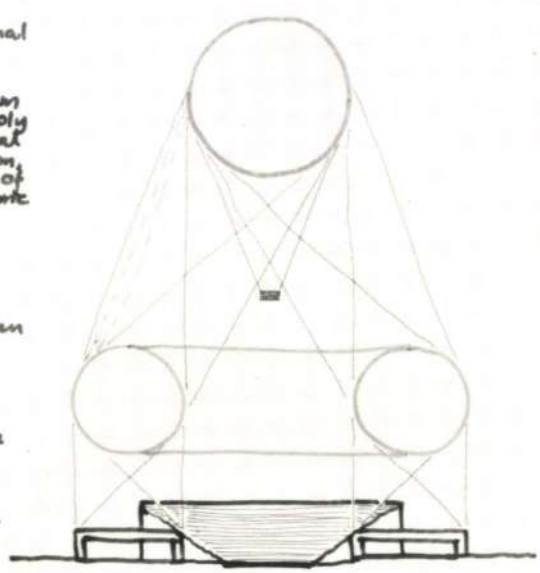

This does, needless to say, require the pavilion to be constantly manned, like a ship or a windmill, but this is considered quite acceptable in a structure of its type.

A gondola, slung under the red balloon, is provided as a control station.

In fine weather, and when no events are taking place in the arena, a second gondola is raised and lowered to offer rides and views to the paying public.

In very severe wind conditions, it may be necessary to lower the red balloon so that it nests within the blue one. This feature has allowed the designers to set an upper limit to the wind forces to be catered for.

When the exposition is over, a useful open air arena will remain.

The balloons can be stored for another day, or simply flown away.

Or cut up and made into masses of French flags of all sizes, to be sold as souvenirs of the 200th anniversary of the Republic and Expo 89.

Arup
IDEAS
Competition

Second prize:
'Paris/Aphrodite'
George Zintilis

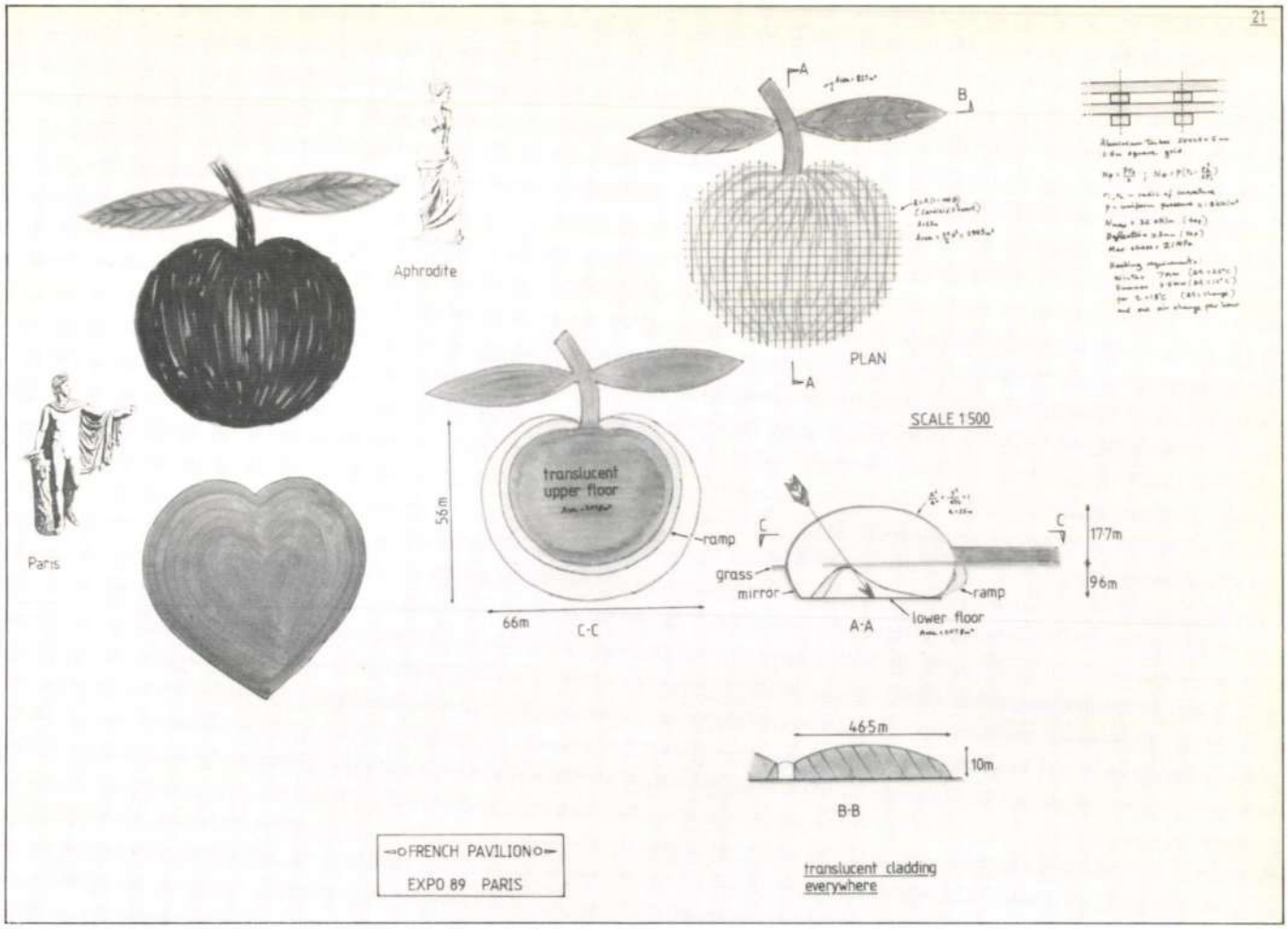

Very sensuous, romantic and French (or at least as the French are popularly seen). In engineering terms, there are uncertainties and contradictions; the strength lies in its softness, colour, texture, form and, to some extent, its symbolism – and less in its engineering. A very beautiful proposal, the only reservation being that the 'apple' might not be perceived at ground level – only from the Eiffel Tower. By far the most seductive of the entries – and one must beware of this sort of seduction. But the drawings convey a convincing feeling for the character and potential of this scheme.

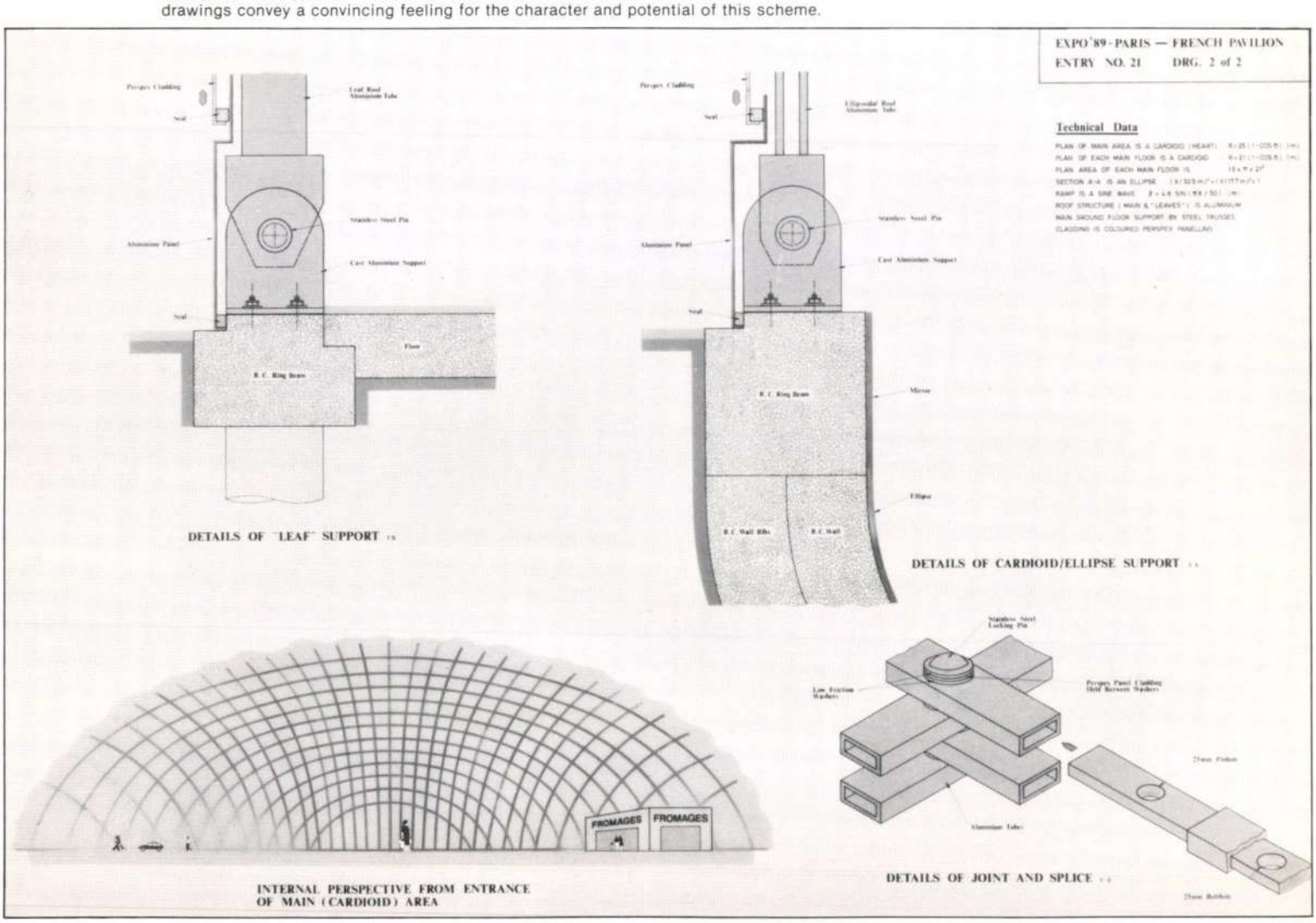

Joint third prize
'Malaysian Umbrellas'
John Eddison

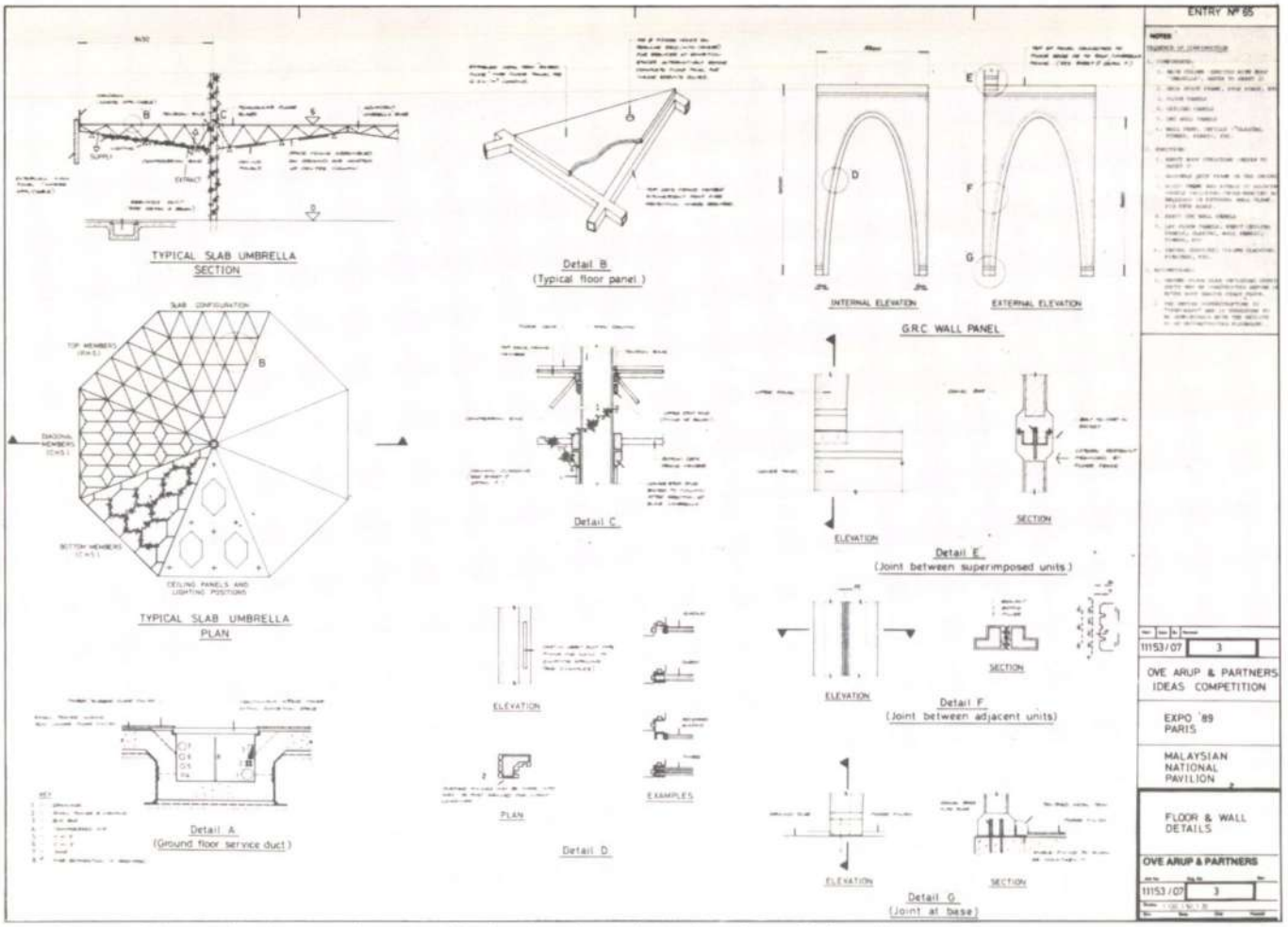

A gentle, non-strident, nationally appropriate entry. The drawings do not flatter the scheme. Perhaps the delicate umbrella structure should have been emphasized, or the umbrellas could have been separated a little more rather than just building up to a dense block. Probably the heavy cantilever floors could have been replaced by a more simple 'lacy' structure to continue the transient character. The tent structure might not open and shut easily. The scheme would make a modest but distinctive and colourful pavilion.

Joint third prize
'All Things'
Chris Jofeh
Ian Smith
Richard Waters

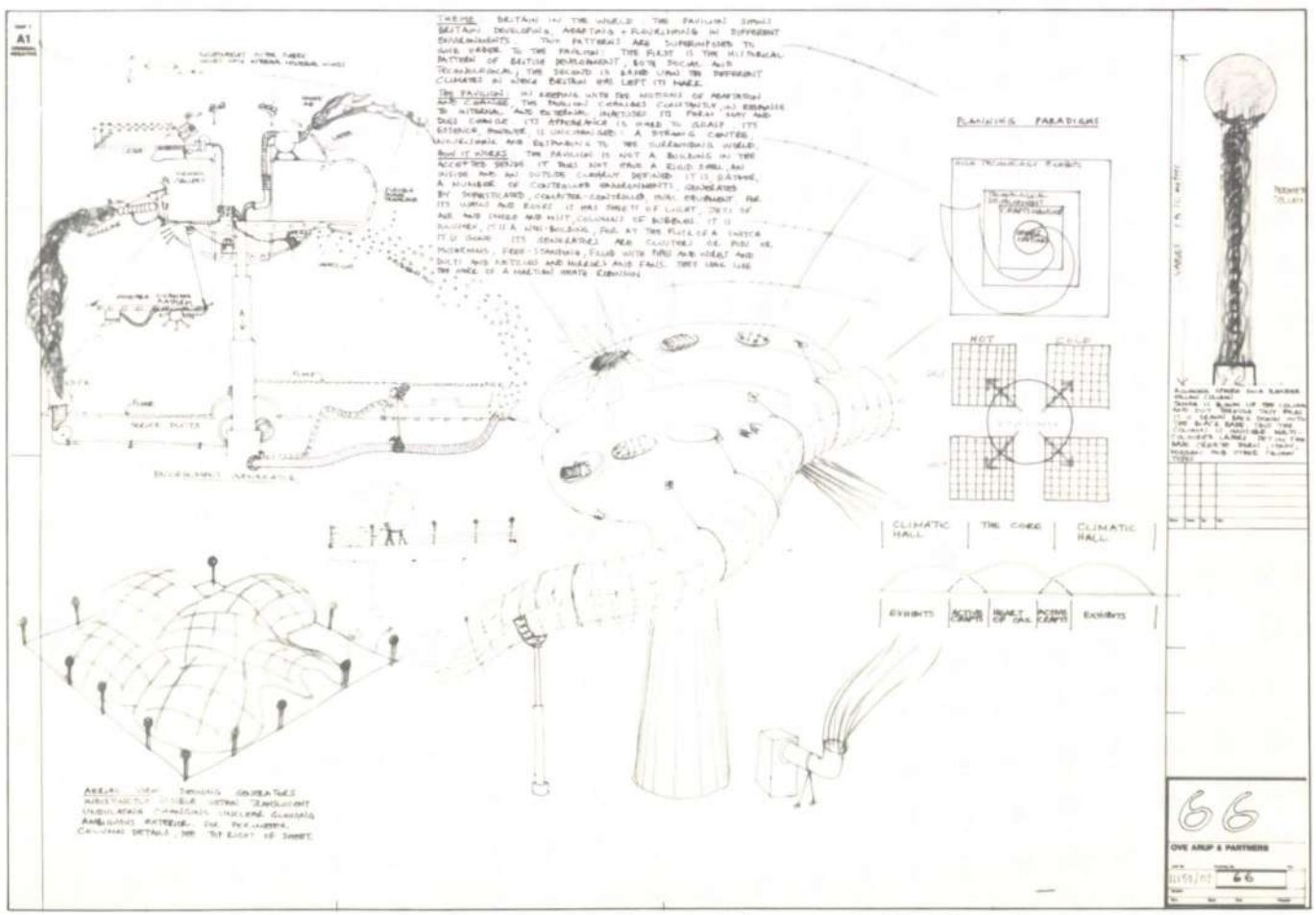

A busy, fizzing-with-ideas, scheme. It is not often that designers consider such simple events as bubble-walls, smoke-screens, etc. The excellent initial entry was better than the final work, which probably ran into trouble when the entrant tried to make a building form. He probably should not have attempted to do this, but just filled several more pages with jottings and non-building ideas. Obviously you cannot delineate adequately such an intangible 'building' – probably there should have been a depiction of a 'frozen moment'. Witty and playful – everything opposite to 'The Tank'; they would make a good combined entry.

Joint third prize
'The Tank'
Ian Gardner

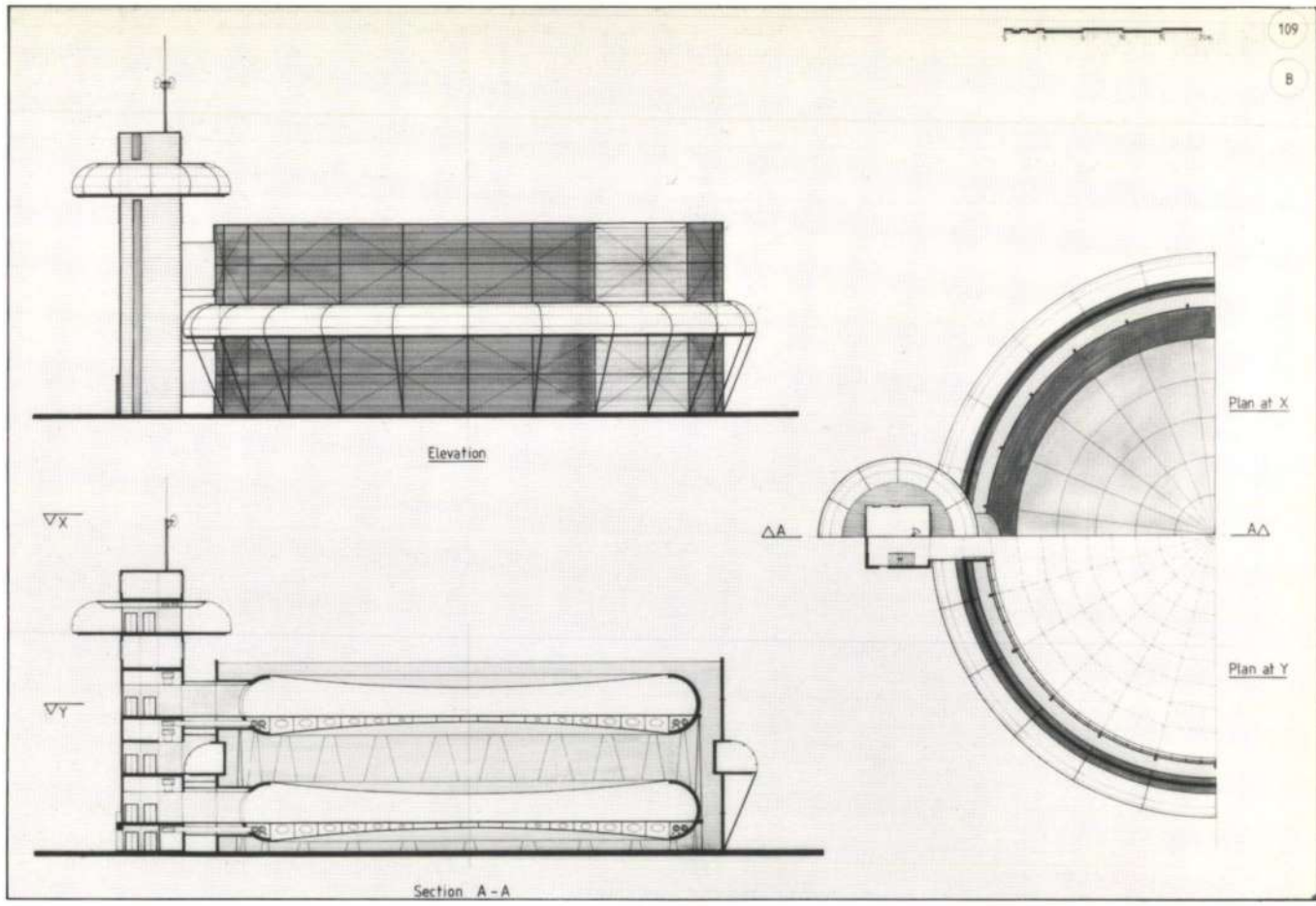

A strong engineering entry looking for some joy and attraction – which should be forthcoming, as essentially the idea of moving around inside tubes inside a tank has potential! A very interesting starting idea but perhaps the public enclosure should not have been so opaque, so that one would know one was under water. Perhaps the 'tube' should have been moored under the Seine.

Joint third prize
'The Containers'
Stuart Richardson

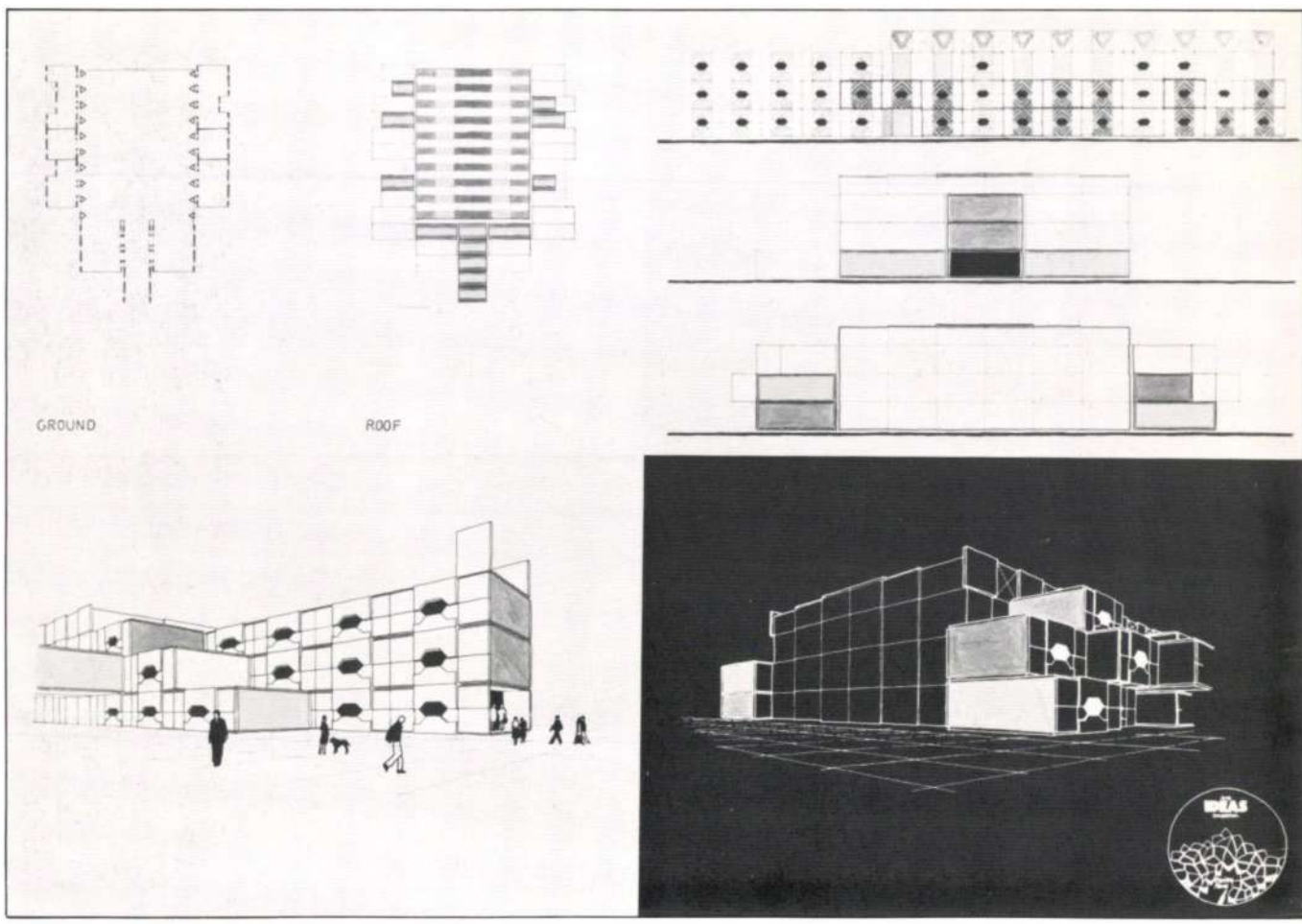

Excellent graphic presentation – probably the best entry in this respect. The engineering concept appears cumbersome and ungainly, but very much to his credit the entrant has in the final building produced an integrated piece of design. Overall there is too much of a packaging concept, not very appropriate for a major Expo pavilion. The building could never live up to the fascination of watching the erection in progress! There is some concern that the ingenuity of the erection system becomes 'mute' once finished. Perhaps too the image is not suitable for an exhibition of several high-tech companies; a little too Meccano.

Book review

Atrium buildings:
development and design
Richard Saxon
Architectural Press 1983

Comments on the chapter on fire safety

Margaret Law

Many people already work or live in buildings that overlook a confined space, which may be a lightwell, courtyard, street or square. Why does placing a roof over the space increase the fire hazard? Alan Parnell and Gordon Butcher, the co-authors of the chapters on design for fire safety in Richard Saxon's book, explain very clearly how smoke can accumulate and fill even a very large enclosed void and spread into any surrounding open-sided accommodation. Many solutions — essentially aiming to prevent smoke entering the atrium, or to let it enter and vent safely to the open air — are described in principle and illustrated by case studies. What is established is that fire safety design should not be based on arbitrary rules: it must take into account how the building is used and the nature of the risks.

Having opened with a description of the challenge of designing fire safety for atrium buildings the chapter continues with a survey of the basic principles of means of escape. The normally accepted travel distances are quoted but their relevance to the type and size of space and the sort of people using the escape routes is not mentioned, which is surprising from authors who, quite rightly, emphasize the importance of design according to the circumstances.

Some production is carefully described in terms of air entrainment into the plume of hot gases produced by a fire and the physics of hot air movement. The calculation methods described do not take into account the actual constituents of the smoke, its toxicity or visibility, but assume that any heated air is hazardous and must therefore be controlled.

Most of the discussion is on smoke control, but some attention is paid to control of internal fire spread. It is pointed out that the risk of floor-to-floor fire spread up the inner face of an enclosed atrium is no different from that at the outer face of any building. It is somewhat startling to read that vertical fire spread is more likely if the floors facing the atrium are glazed, rather than open. When flames from a fire on one floor break out into the atrium they will tend to curve back to the floor above if glazing prevents air getting behind the flame to project it forward. However the glazing, while intact, considerably reduces the radiation transmitted to the interior, and it cannot be assumed that it would always be safer to omit it.

It is a little pessimistic to say that no smoke control is possible without strict and rapid fire-size limitation. For example, the proposals for covering over Basildon Town Square (see *Architects' Journal* 1.6.83, pp.42-53) are based on the assumption that fire size in a shop or office is not limited and grows exponentially until controlled by the fire brigade. There are other large spaces — analogous to the covered railway station which used to be filled with steam engines — which would also be reasonably safe for escape at ground level for some time after the start of a fire even if it did spread.

In general, this chapter gives steady-state solutions, which are likely to be correct for the general range of atrium buildings. However, the transient solution is also of considerable interest, since it takes into account the time for a fire to grow to a certain size, how soon visibility would be impaired and how long it would take to evacuate the space. The authors' smoke control methods assume a sprinkler-controlled fire, of a probability-based design size. It is equally possible to assume a probability-based design size of a non-sprinklered fire.

At present in this country there is little agreement on what size of fire risk we should be designing for in atrium buildings, and what measures are appropriate to deal with it. The only published code is the US NFPA Code 1981 and, although the authors are quite right to point out some of its defects, we should be working towards the production of a UK design guide which is even better. This chapter should certainly stimulate architects and engineers to press for such a guide, and even if that were its only effect it would be valuable. However, it will also be a useful tool to convince clients both here and overseas of the necessity for good fire safety design, and will provide a sensible basis for discussion with the regulatory authorities.

New Gateway House, Basingstoke

An article on this Arup Associates project will appear in a forthcoming issue of *The Arup Journal*

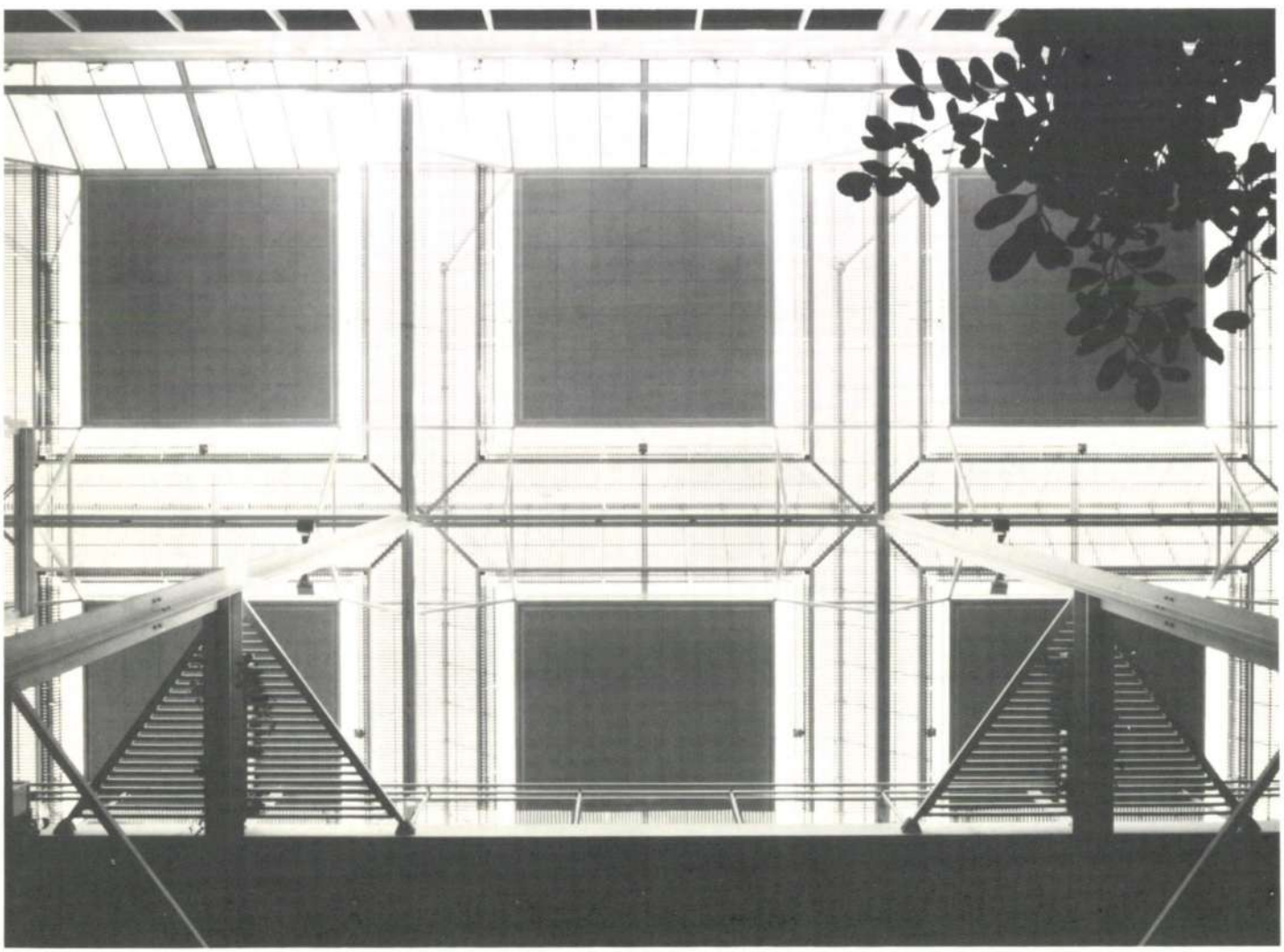

Printed in England by Reedprint Limited, Windsor, Berkshire